frontiers in Earth Science

ORIGINAL RESEARCH
published: 26 November 2019
doi: 10.3389/feart.2019.00311

The Graham Volcanic Field Offshore Southwestern Sicily (Italy) Revealed by High-Resolution Seafloor Mapping and ROV Images

Danilo Cavallaro and Mauro Coltelli*

Istituto Nazionale di Geofisica e Vulcanologia, Sezione di Catania, Osservatorio Etneo, Catania, Italy

The understanding of submarine monogenetic volcanic fields, especially if located near to coastal areas, is fundamental for volcanic risk assessment. Using high-resolution bathymetric data and ROV images, the submarine Graham volcanic field, located 40–50 km offshore southwestern Sicily (Italy), has been described in detail. The field comprises a ten of monogenetic volcanic seamounts aligned along a N-S trending belt at 150–250 m water depths and includes the relict of the short-lived "Ferdinandea Island" produced during the well-documented 1831 "Surtseyan-type" eruption. The present-day morphology of the cones is the result of the interplay between volcanic activity, wave and current erosion, mass-wasting and depositional processes, in relationship with sea-level change, acting in both subaerial and submarine environments. The analysis of the morphometric parameters allowed a detailed morphological classification of the cones. The seamounts are composed of poorly consolidated tephra and show steep slopes and pointy or flat tops, often characterized by sub-vertical knolls. Taking into account analogies with other volcanic seamounts worldwide, the analysis of some morphological characteristics, such as presence and depth of terraces on top and along the slope of the cones in relationship with sea-level fluctuations, allowed us to hypothesize a Late Pleistocene-Holocene age for the volcanism forming the field. The probably older Terribile volcanic field was also identified on the adjacent Terribile Bank and analyzed. Numerous mass-transport deposits and pockmarks were identified in the surroundings of the volcanic fields, suggesting the occurrence of diffuse slope failures and fluid releases, respectively. The distribution and shape of the cones within the volcanic fields provided important insights into the interaction between volcanism and tectonics. The alignment of the cones and the main axis of the clusters in which they are grouped revealed two preferred directions, N-S and NW-SE, respectively, which are consistent with those of the main tectonic structures of the Sicily Channel. The detailed bathy-morphological analysis of the cones proved the monogenetic nature of this volcanism, which represents a peculiarity since it took place outside the typical geodynamic settings of other volcanic fields worldwide such as subduction or oceanic rift zones, and far from long-lived volcanic systems.

Keywords: submarine volcanism, volcanic field, submarine terraces, bathymetric data, ROV images, Surtseyan-type eruption, Ferdinandea Island, Graham Bank

OPEN ACCESS

Edited by:
Guido Giordano,
Roma Tre University, Italy

Reviewed by:
Dario Pedrazzi,
Instituto de Ciencias de la Tierra Jaume Almera (ICTJA), Spain
Claudia Romagnoli,
University of Bologna, Italy

****Correspondence:***
Danilo Cavallaro
danilo.cavallaro@ingv.it

Specialty section:
This article was submitted to Volcanology, a section of the journal Frontiers in Earth Science

Received: *07 April 2019*
Accepted: *08 November 2019*
Published: *26 November 2019*

Citation:
Cavallaro D and Coltelli M (2019) The Graham Volcanic Field Offshore Southwestern Sicily (Italy) Revealed by High-Resolution Seafloor Mapping and ROV Images. Front. Earth Sci. 7:311. doi: 10.3389/feart.2019.00311

INTRODUCTION

Monogenetic volcanic fields occur in several areas worldwide and within different geodynamic settings such as subduction, intraplate and rift zones (Kereszturi and Németh, 2012; Cañón-Tapia, 2016). Nevertheless, they are mostly associated with extensional regimes and sometimes are located along transfer zones (e.g., Camargo volcanic field, Chihuahua, Mexico, Aranda-Gómez et al., 2003). Monogenetic volcanic fields are generally isolated from large composite volcanoes, however, they can form in the immediate surroundings of long-lived volcanic systems such as major calderas, stratovolcanoes and shield volcanoes, in both subaerial and submarine environments. While individual volcanoes within the fields have geologically short life spans and are generally monogenetic, the fields themselves can be active for several million years (Németh, 2010; Valentine and Connor, 2015). A monogenetic basaltic volcanic field may comprise from tens to hundreds of individual volcanic centers, generally erupting a small volume of magma (typically $< < 1$ km^3) as both pyroclastic products and lava flows (Németh and Kereszturi, 2015). Individual volcanic centers within a field are commonly arranged to form clusters and alignments, attesting a control by underlying tectonic structures and stress regime (Németh, 2010; Cañón-Tapia, 2016).

Underwater monogenetic volcanic fields are located on both deep and shallow waters. They often develop on ocean ridges, such as those identified within the Azores Archipelago (Casalbore et al., 2015) or near Easter Island in the southeastern Pacific (Rappaport et al., 1997), on subduction zones like the Aegean Volcanic Arc (Foutrakis and Anastasakis, 2018) and in intraplate setting such as those surrounding Canary Islands (Romero Ruiz et al., 2000) or Bridge Point-Aorere Point volcanic center, offshore Otago, New Zealand (Cas et al., 1989). Shallow water submarine volcanic fields are usually originated by hydromagmatic eruptions known as "Surtseyan-type" (Kokelaar, 1983; White and Houghton, 2000), bearing the name from the 1963–67 eruption, which began at about −140 m, generating the small island (Surtsey) off South Iceland (Thorarinsson, 1967; Kokelaar and Durant, 1983). These explosive eruptions are characterized by the formation of small- to medium-size scoria cones, and generally, their intensity is progressively restricted with increasing water depth (Cas and Giordano, 2014). Recent shallow submarine volcanic activity also occurred at Capelinhos (Machado et al., 1962) and Baixa da Serreta Bank (Weston, 1964), offshore the Azores Islands; Kavachi volcano, Solomon Islands (Baker et al., 2002); Hunga Haapai, Tonga (Vaughan and Webley, 2010); offshore El Hierro, Canary Islands (Rivera et al., 2013); Socorro Island, offshore Mexico (Siebe et al., 1995); Nishima-Shima, Izu Volcanic Arc, Japan (Global Volcanism Program, 2013b).

The morphology of underwater volcanic edifices, especially if forming islands, since their formation and during their evolution, is strictly controlled by the competition between constructive (volcanic and depositional activity) and destructive processes (such as wave and current erosion, mass-wasting and subsidence) acting both in subaerial and submarine environments (Ramalho et al., 2013; Romagnoli and Jakobsson, 2015). This is particularly important for short-lived cones made by pyroclastic rocks (White, 1996). Primary controls on the shape of volcanic seamounts are: tectonic setting; effusion rate and magma physical properties (mainly viscosity and gas content); shape, size and geometry of magma supply conduits; age and thickness of the lithosphere; thermal and compositional heterogeneities of the mantle, depth of the eruption site (Rappaport et al., 1997 and references therein). Water depth is one of the main controls of submarine eruptions since the hydrostatic pressure generally inhibits the amount of magma erupted and the explosivity of the eruption (Kokelaar, 1986; White, 1996; Cas and Giordano, 2014).

Once volcanic processes end, the scoria cones emerging above sea level are rapidly affected by wave-current erosion, resulting in formation of shoals; therefore, the existence of surtseyan cones maybe ephemeral (Schmidt and Schmincke, 2002).

Submarine volcanic cones within fields show a variety of morphologies ranging from pointy to flat-topped cones. The pointy cones reflect the lack of wave erosion processes affecting their summits, suggesting that they have not reached the near sea-surface during their life cycle. Conversely, the flat-topped cones can be formed either by wave-dominated erosive activity at wave base level (Cas et al., 1989; Trenhaile, 2000; Schmidt and Schmincke, 2002) or by lava infillings of early stage summit craters or calderas (Clague et al., 2000b), or else as continuously and long-lasting overflowing submarine lava ponds (Clague et al., 2000a). Moreover, many cones, during and after the time they were erupting often exhibit hydrothermal activity, highlighted by the presence of pockmark and fumarole fields.

The post-emplacement morphology of seamounts reflects several other processes, which interplay in a complex manner to modify their present-day shape: isostatism, tectonic deformation (e.g., uplift or subsidence), hydrothermal activity, subsidence due to compaction, slope failures, lithology and mechanical properties of the volcanic products, amplitude of eustatic change, wave and currents parameters, coral reef growth and biogenic production (Ramalho et al., 2013 and references therein).

Generally, on volcanic islands, particularly of polygenetic origin and recent formation, the timing and magnitude of relative sea-level change can be difficult to evaluate due to the possible occurrence of crustal vertical deformation induced by long-term regional tectonic and short-term volcano-tectonic processes (Lucchi et al., 2019). However, for scattered small monogenetic volcanic cones, as is the case of those forming a volcanic field, the deformation induced by volcanic processes are highly attenuated because of the lack of any long-lived volcanic center, plumbing system, magmatic reservoir, etc.; the subsidence for compaction is also minimized because of the generally low amount of pyroclastic material.

Summit abrasion platforms and submarine terraces result mainly from the combined work of wave erosion and sea-level change, and so their width and maximum depth experienced adjustments depending on the variability of the sea oscillations (Trenhaile, 1989, 2001). Summit abrasion platforms and submarine volcanoclastic terraces (SDTs) can be used, if supported by data on the vertical mobility affecting the area, as proxies for reconstructing relative sea-level positions with the purpose of constraining the age of the associated volcanism

(Casalbore et al., 2017). In particular, the depth of the summit abrasion platforms of truncated cones can be used to likely infer the age of the erosive activity flattening them, and thus may furnish a tool to reconstruct relative sea-level positions, taking into account the analogy with the present-day wave erosion level. Similarly, the inner margin of a marine terrace bounded by a paleo-cliff can be considered as a proxy of the shoreline position at the time of its formation.

SDTs are terrace-shaped sedimentary prograding wedges, found at variable water depths on continental and insular shelves characterized by high-energy marine settings. Their formation is associated with the downward transport of sediments from the surf zone and shoreface in stormy conditions during a highstand (interglacial) sea level peak (Hernàndez-Molina et al., 2000; Casalbore et al., 2017). The depositional edges (or rollover depth, Mitchell et al., 2012a) of the present-day SDTs lie at depths approximating the modern local storm-wave base level, and vary between 15 and 60 m bsl in the different areas of the world depending on the different wave climate conditions (in the western Mediterranean they were measured at about −32 m by Mitchell et al., 2012a, while in the Tyrrhenian Sea at 10–30 m below sea level (bsl) by Casalbore et al., 2017). Thus, they can be used for paleo sea-level estimation as modern analogs for relict terraces having depositional edges at greater depths, formed in the past (after the LGM – Last Glacial Maximum), when the sea level was lower, as well as to estimate local vertical movements (Casalbore et al., 2017).

Since volcanic activity in shallow water may result in explosive eruptions (Kokelaar and Durant, 1983) and tsunami generation (Latter, 1981), improving the knowledge of time-space activity forming submarine monogenetic volcanic fields, especially if located close to coastal areas, would be of great interest for volcanic risk assessment, which is mostly associated with the local navigation.

Based on multibeam echo-sounder data, Coltelli et al. (2016) recognized a small submarine volcanic field (hereby-named Graham volcanic field, GVF) in the surroundings of the Graham Bank (northwestern portion of Sicily Channel, Italy), the place of the 1831 submarine eruption, which originated the ephemeral "Ferdinandea Island." In this study we present a new detailed bathy-morphological analysis of the cones composing the GVF with particular reference to the Ferdinandea shoal being the youngest of the field. Ferdinandea cone represents a well-documented example of a previous island turning into a seamount. Since its formation, "Ferdinandea Island" has suffered a strong wave and current erosive activity causing its rapid submersion, which substantially modified its original shape. The bathy-morphological analysis of another volcanic field (hereby-named Terribile volcanic field, TVF), identified on the near Terribile Bank, was also carried out.

In order to prove the monogenetic nature of the volcanism originating the fields, the relationship between the morphology of the seamounts and underwater volcanic processes was studied. Another goal was to verify a potential interaction between volcanism and tectonics in the formation and distribution of the seamounts within the volcanic field through an analysis of the main direction of the clusters in which they were grouped. For the same aim, since the ellipticity of the base of cones is often influenced by the direction of the main stress axis acting at time of their formation (Tibaldi, 1995; Corazzato and Tibaldi, 2006; Németh, 2010), a morphologic classification, focused on measuring the main dimensions and morphometric associated parameters of the seamounts, was carried out.

Finally, we inferred the possible age of formation of GVF, by comparing the post-eruptive morphological characteristics of other short-lived pyroclastic cones worldwide (such as the satellite volcanic centers formed during the 1963 eruption at Surtsey; Romagnoli and Jakobsson, 2015) to the Ferdinandea seamount and then to the other seamounts of the field in relationship with sea-level change.

This study may also provide a key to better understand the volcano-tectonic setting of this region and furnish a useful comparison for other submarine areas affected by monogenetic volcanism.

GEOLOGICAL SETTING

The study area is located in the northwestern sector of the Sicily Channel, Central Mediterranean Sea (**Figure 1**). The Sicily Channel belongs to the northern margin of the African continental plate, called the Pelagian Block (Burollet et al., 1978), which corresponds to the foreland area of the Sicilian sector of the Apenninian-Maghrebian fold-and-thrust belt. Its geodynamic setting is the product of the Neogene collision between the African and European plate margins associated with the NW-SE oriented Late Miocene–Quaternary continental rifting, which produced the Pantelleria, Linosa, and Malta grabens (Jongsma et al., 1985; Boccaletti et al., 1987; Reuther et al., 1993). The Sicily Channel consists of a 6–7 km thick Mesozoic-Cenozoic shallow- to deep-water carbonate sedimentary successions with repeated intercalations of volcanic deposits, covered by Upper Tortonian-Lower Messinian siliciclastic deposits and Plio-Quaternary clastic sequences (Torelli et al., 1995).

The northern side of the Sicily Channel is characterized by a very uneven bathymetry, being a composite array of shallow continental shelves (the Siculo-Maltese Shelf and the Adventure, and Malta plateau), deep depressions, such the fault-controlled Pantelleria, Linosa, and Malta grabens and a foredeep depocenter (the Gela Basin), and topographic highs, such us several small- to middle-scale banks of sedimentary origin (e.g., the Nerita, Terribile, Nameless, and Madrepore banks) (Colantoni, 1975; Calanchi et al., 1989; Cavallaro et al., 2017; **Figure 1**). Within the Sicily Channel, a widespread and scattered volcanism is known to have occurred during Upper Miocene to Pleistocene times, building up the alkaline volcanic islands of Linosa and Pantelleria and several other volcanic centers (e.g., Anfitrite, Tetide Galatea, Cimotoe banks) (Beccaluva et al., 1981; Calanchi et al., 1989; Rotolo et al., 2006; Civile et al., 2008, 2015; Lodolo et al., 2012, 2019a,b; Pensa et al., 2019; **Figure 1**). Volcanism occurred up to historical times, with the 1831 submarine eruptions of Ferdinandea Island (Gemmellaro, 1831; Marzolla, 1831; Colantoni et al., 1975; Dean, 1980) and the 1891 eruption off NW Pantelleria Island (Washington, 1909;

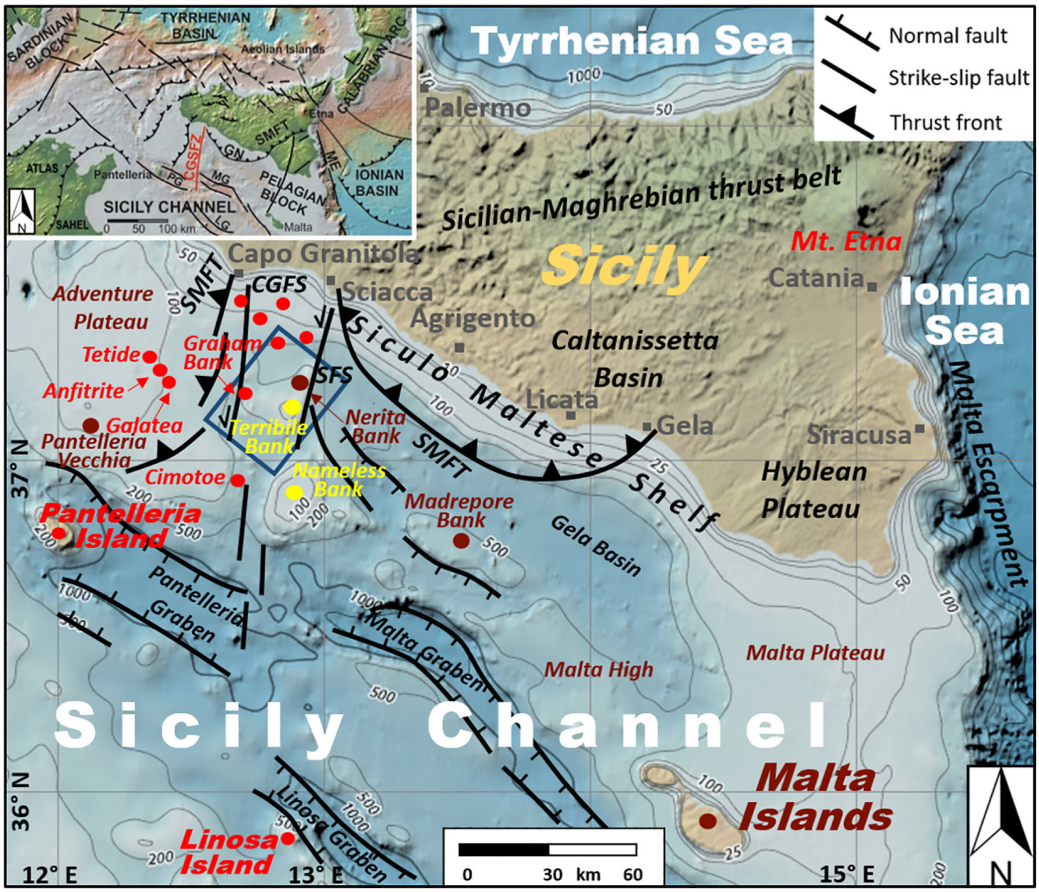

FIGURE 1 | Shaded-relief bathymetric map of the northern portion of the Sicily Channel (from GEBCO-General Bathymetric Chart of the Oceans-Digital Atlas). The blue box shows the study area; the red, brown and yellow circles indicate the location of volcanic centers, sedimentary banks and sedimentary banks with scattered volcanic manifestations on top, respectively (from Calanchi et al., 1989; Civile et al., 2015, 2018; Lodolo et al., 2019a). CGFS, Capo Granitola fault system; SFS, Sciacca fault system; SMFT, Sicilian–Maghrebian fold-and-thrust belt front (from Civile et al., 2018). The inset shows the geodynamic setting of the Central Mediterranean; GN, Gela Nappe; ME, Malta Escarpment; PG, Pantelleria Graben; LG, Linosa Graben; MG, Malta Graben; CGSFZ,Capo Granitola-Sciacca Fault Zone (from Civile et al., 2018).

Conte et al., 2014). Some of these volcanic centers are sited in an area extending from the Adventure Plateau to the Nameless Bank, informally known as the "Campi Flegrei del Mar di Sicilia" (Global Volcanism Program, 2013a).

The volcanic centers of the GVF, those on the Nameless Bank and in the nearshore of Capo Granitola-Sciacca coast, together with Cimotoe volcanic seamount (Civile et al., 2015, 2018; Coltelli et al., 2016; Lodolo et al., 2019a), are aligned along a nearly N-S oriented belt extending southwards for almost 200 km up to Linosa Island. This belt was related to a lithospheric-scale transpressive transfer zone (the Capo Granitola-Sciacca Fault Zone, CGSFZ; see inset in **Figure 1**) between the western and eastern sectors of the Sicily Channel Rift Zone, characterized by different amount of rifting (Argnani, 1990; Civile et al., 2014, 2018). The CGSFZ is also positioned between two tectonically independent sectors of the offshore part of the Sicilian-Maghrebian Chain, characterized by different deformation ages, structural trends and tectonic evolution, playing a key role in the Neogene-Quaternary geodynamic evolution of the region (Argnani, 1990; Corti et al., 2006; Civile et al., 2008, 2014, 2018; Ghisetti et al., 2009; Calò and Parisi, 2014; Cavallaro et al., 2017; Fedorik et al., 2018; Ferranti et al., 2019). The CGSFZ is composed of two major left-lateral strike-slip systems: the Capo Granitola fault system (CGFS) to the west, which affects the GVF area, and the Sciacca fault system (SFS) to the east (**Figure 1**), which bounds the eastern extent of the Nerita and Terribile banks (Civile et al., 2018; Fedorik et al., 2018; Ferranti et al., 2019). Ferranti et al. (2019), based on seismic reflection profiles, inferred that folds and faults offshore Capo Granitola and Sciacca are different scale expression of the CGFS and SFS, which were active in left transpression since the Latest Miocene-Early Pliocene and are still active; transpressional deformation along the southern segments of the CGFS and SFS inverted the previous Late Tortonian-Early Messinian extensional or transtensional basins with an uplift rate of about 2 mm/yr during the Plio-Quaternary. The CGSFZ is also characterized by moderate seismicity (Coltelli et al., 2016) with large seismic

gaps in the proximity of the Graham Bank, associated with the geothermal and volcanic activity (Calò and Parisi, 2014), and by remarkable magnetic anomalies (Colantoni et al., 1975; Lodolo et al., 2012).

Other volcanic seamounts are arranged to form minor clusters with different orientations, like the three small volcanic shoals, Tetide (summit depth at −18 m), Anfitrite (−35 m) and Galatea (−74 m), located on the Adventure Plateau along a nearly 10 km long NW-SE oriented alignment (Calanchi et al., 1989; Civile et al., 2014, 2015; Pensa et al., 2019; **Figure 1**).

Despite such diffuse volcanism affecting the northern Sicily Channel, no quaternary volcanism occurs onshore in south-west Sicily.

The study area includes three banks: Nerita, Terribile and Graham (**Figures 1**, **2**).

The Nerita Bank is a morphological high, elongated in a NNE-SSW direction (**Figure 2**). On the basis of seismic reflection profiles, it was interpreted as an almost symmetrical push-up structure of carbonate origin, generated along strike-slip tectonic faults (i.e., SFS), lacking volcanic structures on it (Argnani, 1990; Civile et al., 2015, 2018; Fedorik et al., 2018).

The Terribile Bank is a carbonate submarine plateau (Colantoni, 1975), with several small conical-shaped structures on top (**Figure 2**); seismic profiles indicate that it is made of an Upper Cretaceous-Eocene to Lower Miocene carbonate succession, overlapped to the west by Tortonian-Messinian sediment missing the Pliocene-Quaternary sequence (Civile et al., 2018).

The Graham Bank includes two volcanic seamounts, the smallest of which is the relict of the short-lived "Ferdinandea Island," originated during the 1831 Surtseyan-type eruption, which represents the only well-documented volcanic event occurred in the study area; other volcanic activities were uncertainly reported in the surroundings of Graham Bank during the first Punic war (264-241 BC) (Guidoboni et al., 2002; Bottari et al., 2009), in 1632, 1833, and 1863 (Antonioli et al., 1994; Falzone et al., 2009). Moreover, numerous episodes of strong gas releases in the Graham Bank area were observed in 1816 (Mercalli, 1883), 1845, 1942 and more recently in 2003.

The emersion and disappearance of the island during and after the 1831 submarine eruption are well-described in literature (Gemmellaro, 1831; Marzolla, 1831; Dean, 1980). The eruption was preceded, between the end of June and the first days of July 1831, by an intense seismic activity, which produced damage in the Sciacca area. On July 16–17 the island emerged; during the following weeks it grew up rapidly in size, reaching 600 m in diameter and about 60 m in height. The eruption ceased on August 16, after about 6 weeks of activity. During the following months, the island was rapidly dismantled by the sea: at the end of September it was some 20 m high; 1 month later it consisted of a less than a one-meter-high islet, and finally, between December 1831 to January 1832, it completely disappeared. Two bathymetric surveys carried out in 1883 and 1914 by the Istituto Idrografico Regia Marina described the top of the shoal at 3 and 8 m bsl, respectively (Falautano et al., 2010). While the bathymetric survey carried out in 2012 (this paper) and those in 2012 and 2014 by the Istituto Idrografico della Marina (IIM) (Sinapi et al., 2016) measured the top at about 9 m bsl.

Dredged rocks from the Graham Bank consist mainly of poorly evolved alkali basalts (Calanchi et al., 1989; Rotolo et al., 2006). A piece of a palagonitized tephra layer was sampled at the base of the northern side of the Graham Bank, likely representing the consolidated deposit of the final surtseyan explosive activity of the 1831 eruption (Coltelli et al., 2016).

The composition of a gas sample, collected within a fumarole filed at 155 m water depth near the base of the eastern cone of the Graham Bank, revealed a significant mantle component; helium and carbon isotope compositions of gas emitted from the seafloor reflect a clear magmatic/crustal origin (Coltelli et al., 2016). Petrological data suggest that all the volcanic centers of the Sicily Channel lack a shallow-level magma chamber, where primitive magmas could pond and fractionate and crustal contamination is generally absent (Rotolo et al., 2006).

Finally, in the proximity of the GVF, three deposits of dead red coral have been discovered (Di Geronimo et al., 1993). They may have accumulated, during the post-LGM, as consequence of periodic collapses, possibly associated with volcanic and/or seismo-volcanic activity, dislodging living (or dead) corals from the steep flanks of volcanoes on which they lived (Di Geronimo et al., 1993; Lodolo et al., 2017).

MATERIALS AND METHODS

The dataset used for this work consists of multibeam bathymetric data and Remotely Operated Vehicle (ROV) images. Data were collected during the multidisciplinary oceanographic cruise "Ferdinandea 2012" carried out in 2012 by INGV (Istituto Nazionale di Geofisica e Vulcanologia) offshore southwestern Sicily on the Research Vessel Astrea of ISPRA (Istituto Superiore per la Protezione e la Ricerca Ambientale) (Coltelli et al., 2016). The latter paper focused on the preliminary results of the oceanographic cruise giving a short and general description of the main morpho-structural features of the area, describing seafloor and gas samples and the local underwater seismic monitoring, which was carried out by means of OBS/Hs (ocean bottom seismometer with hydrophone). The high-resolution seafloor mapping covered an area of nearly 70 km^2, focusing on the GVF (**Figures 1**, **2A,B**). It was performed by using an EM 2040 Kongsberg multibeam sonar system with a frequency range of 200–400 kHz supported by GPS-RTK positioning. SIS software by Kongsberg was used for data acquisition. Daily sound velocity profiles and repeated calibration of transducers were applied to get the best possible data resolution. CARIS Hips & Sips software package was utilized for data processing (calibration and processing of navigation, correction for sound velocity and tide variation, noise filtering and removal of erroneous beams), producing a very high-resolution Digital Terrain Model of the seafloor, with a bin size of 5 m, which, for some peculiar areas (e.g., the Ferdinandea seamount), reached 0.7 m. The bad sea conditions during the survey created wave-like artifacts on the bathymetries, somewhere still visible, despite noise

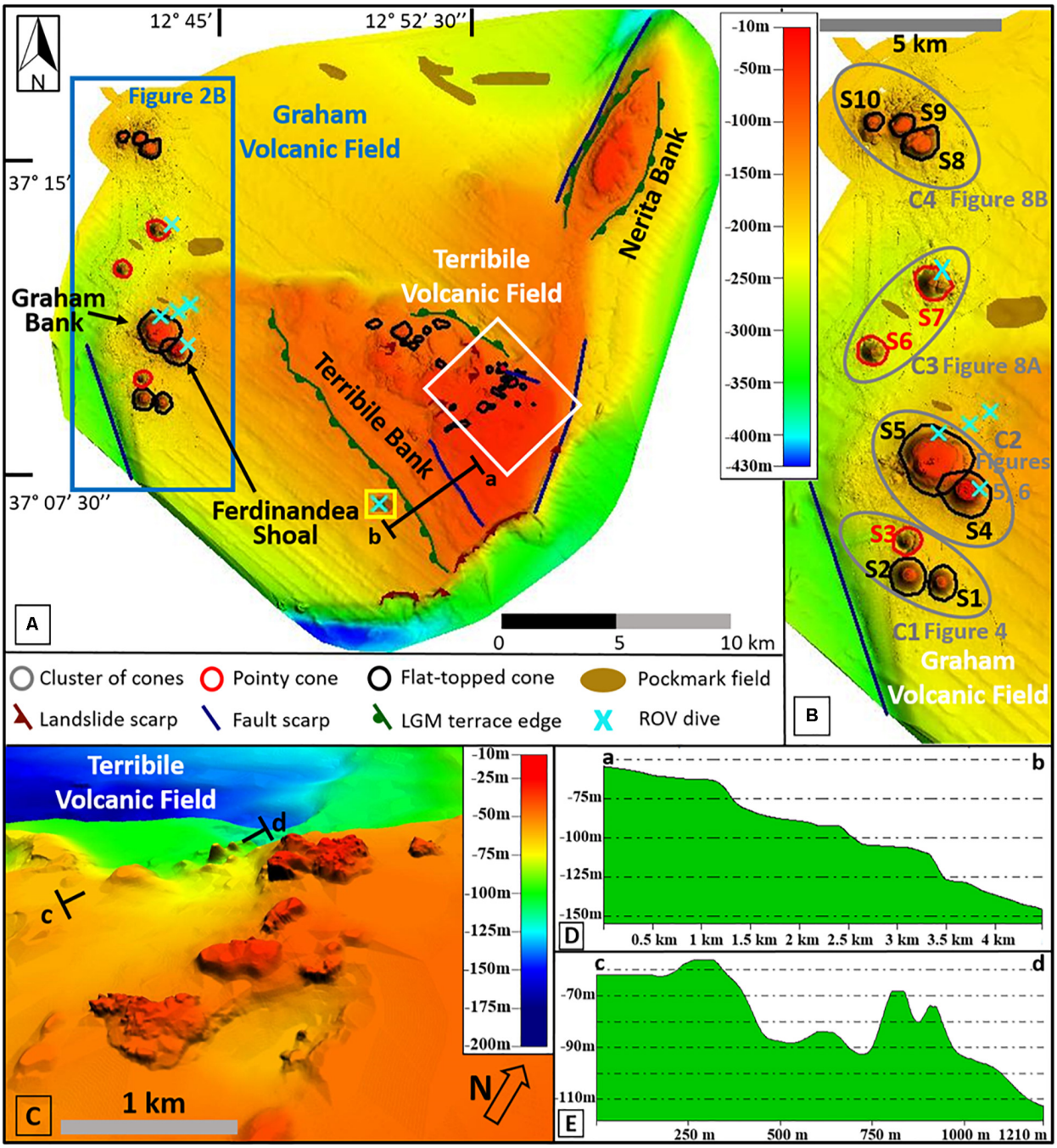

FIGURE 2 | (A) Bathymetry map of the study area displaying the Graham, Nerita and Terribile banks. The blue box shows the GVF, which is zoomed with higher resolution on **(B)**; here the clusters of cones displayed in the next figures are indicated. The small yellow box images the area where the large pockmark of **Figure 3** is located. The white box shows the eastern portion of the TVF, which 3D (vertical exaggeration is 4x) shaded relief image is displayed in **(C)**. **(D)** Bathymetric profile (ab) displaying the steps arrangement of the southwestern portion of Terribile Bank with four terraced areas, whose edges lie at about 130, 105–110, 85–90, and 60 m bsl. **(E)** Bathymetric profile (cd) displaying an alignment of small volcanic cones on top of Terribile Bank.

filtering, and more apparent on the 3D views of smooth surfaces because of the high vertical exaggeration. Our bathymetry was merged with lower resolution bathymetric data related to the Nerita and Terribile banks (about 600 km^2), courteously provided by the IIM.

Furthermore, the repeated bathymetric surveys (single- and multi-beam echo sounders data) carried out from 1890 to 2014 by IIM (Sinapi et al., 2016), together with those realized in 1883 and 1914 by the Istituto Idrografico Regia Marina and that in 1972 by Consiglio Nazionale delle Ricerche

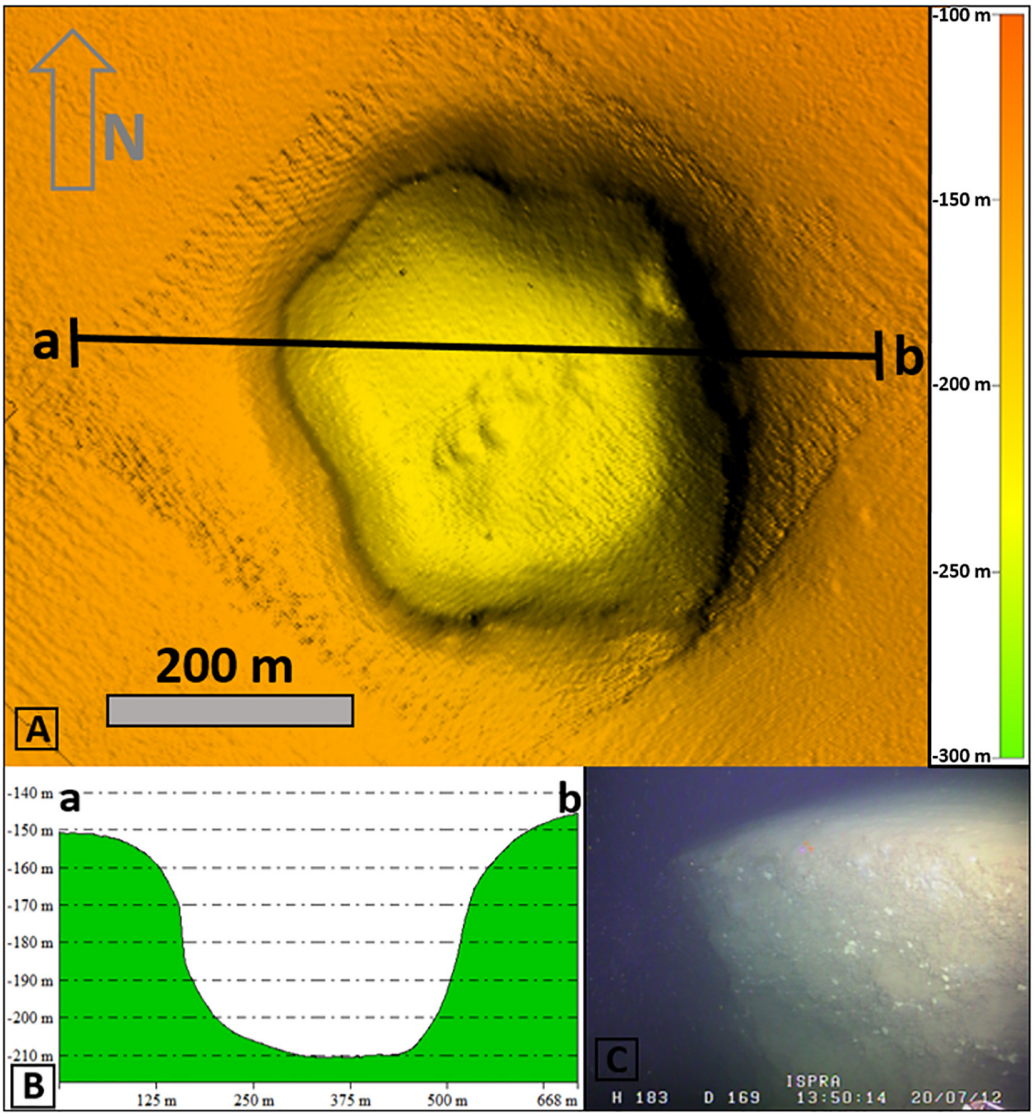

FIGURE 3 | (A) High-resolution shaded-relief image displaying a large pockmark south of the Terribile Bank (location in **Figure 2**). **(B)** Bathymetric profile across the pockmark well displays its sub-vertical and deep walls imaged in the ROV photo of **(C)**.

(Falautano et al., 2010), allowed us to estimate, even if by means of old and low-quality measurements, the depth changes of the summit abrasion platform of the Ferdinandea cone, in order to compare its post-eruptive morphological evolution with that of the others of the field.

Following the definition by Wessel et al. (2010), "Seamounts are active or extinct undersea volcanoes with heights exceeding about 100 m," we interpreted the cones within the GVF as seamounts. Moreover, since their tops lie in shallow water, we also referred to them as shoals.

For the morphological analysis used to describe the cones of the GVF, we adopted the following criterion. Based on the spatial separation between the cones (Cañón-Tapia, 2016), all the seamounts were grouped in clusters. For each volcanic seamount, we indicated location (in geographic coordinates) and local name, if already known. The main morphometric parameters, including summit depth, minimum and maximum basal diameters, cone height, slope gradients and basal area, were measured (**Table 1**). In order to avoid overestimation in case of steep basal surfaces, cone height and width were determined by fitting a line to the inflection points on either side of each cone profile using the method proposed by Mitchell et al. (2012b), as illustrated in **Supplementary Figure S3**; the height of the cone has been measured as the elevation difference between the peak and the basal plane of the cone reconstructed through bathymetric profiles. Unfortunately, the cone bases were not easily identified everywhere because of the presence of talus and/or erosive features. Moreover, the gradient changes locally, and thus the topography can be confused by rugged pre-existing reliefs; hence, individual measurements could have been

TABLE 1 | Main morphological dimensions and morphometric associated parameters of the cones of the GVF.

Cluster id (local name)	Seamount id (local name)	Lat	Long	Cone shape	Summit depth (m bsl)	H (m)	Summit terrace depth (m bsl)	Max D (m)	Min D (m)	Average D (W) (m)	Basal ratio	Basal shape (Max axis direction)	BS (Km^2)	H/W aspectratio	Volume (Km^3)	Average slope gradient (°)
C1	S1	37° 08′ 55″ N	12° 42′ 46″ E	FT	76	117	90–100	870	710	821	1.22	C	0.45	0.14	0.033	26
	S2	37° 09′ 00″ N	12° 42′ 11″ E	FT	66	144	90–100	1050	870	924	1.20	C	0.67	0.16	0.045	25
	S3	37° 09′ 27″ N	12° 42′ 10″ E	P	105	100	/	800	680	730	1.17	C	0.38	0.14	0.018	27
C2 (Graham Bank)	S4 (Ferdinandea)	37° 10′ 10″ N	12° 42′ 09″ E	FT	9	141	25–30	1450	1050	1220	1.38	E (N130)	1.17	0.12	0.056	29
	S5 (Secca del Corallo)	37° 10′ 35″ N	12° 42′ 34″ E	FT	33	137	50–60	1850	1780	1807	1.04	C	2.40	0.07	0.169	18
C3	S6	37° 12′ 04″ N	12° 41′ 28″ E	P	122	118	/	750	720	731	1.04	C	0.42	0.16	0.028	24
	S7 (Secchitella)	37° 13′ 03″ N	12° 42′ 28″ E	P	98	132	/	990	780	874	1.27	E (N115)	0.60	0.15	0.041	23
C4 (Bancazzo)	S8	37° 14′ 57″ N	12° 42′ 14″ E	FT	83	113	85–95	1280	900	1022	1.42	E (N122)	0.82	0.11	0.058	26
	S9	37° 15′ 12″ N	12° 41′ 55″ E	FT	75	109	80–90	1345	750	855	1.79	E (N55)	0.57	0.13	0.035	24
	S10	37° 15′ 14″ N	12° 41′ 23″ E	FT	83	88	90–95	1020	710	821	1.44	E (N30)	0.53	0.11	0.031	23
MEDIAN						120				980			0.80	0.13	0.051	24

FT, Flat-topped; P, Pointy; C, Circular; E, Elliptical; D, Diameter; BS, Basal surface; H/W, aspect ratio (height vs. average basal diameter).

affected by significant uncertainty. These parameters were used to obtain the aspect ratio (height vs. average basal diameter, H/W) of the cone, a morphometric index widely used in both subaerial (Favalli et al., 2009) and submarine (Mitchell et al., 2012b) settings to characterize volcanic cones. The volume of the seamounts was also estimated by using gridded bathymetric profiles and apposite tools of dedicated software. In some locations, individual seamounts consist of overlapping cones, making classification with these parameters difficult. The overlapping basal area represents a minor component of the total area, thus, according to Rappaport et al. (1997), overlapping regions were reasonably included in the basal area of both adjacent seamounts. The same *modus operandi* was used for measuring the cone diameters and volume.

Based on their summit morphology, the cones were divided into two main types: pointy or flat-topped (flattened and/or truncated) cones. Average slope gradient was calculated by averaging the slope gradients of lines connecting the border of the basal plane with the cone top (if pointy cones) or with the border of the summit terrace (if flat-topped cones).

Finally, we classified the basal shape of the cones as circular if the Max axis/Min axis ratio = 1.0–1.25, and elliptical if it is >1.25. This classification is important to define a possible tectonic control, even if the shape of the seamounts also depends on erosive and depositional activity of the post-emplacement processes, which are, in turn, subject to the local wave-current conditions.

We used the depth of the wave-cut summit platforms of the different flat-topped cones within GVF, which is related to the local wave erosive level, as a marker of relative paleo sea levels (e.g., LGM and younger stillstands during the last sea-level rise), with the purpose of inferring the possible age of the volcanism creating the cones of the field, taking into account data on the vertical mobility affecting the area. Similarly, even thought the position of the SDTs' depositional edges (or rollover depth, Mitchell et al., 2012a) is not a direct measure of paleo sea-level positions, because their depth depends on a complex interplay of several factors (such as the storm-wave base level and the occurrence of subsequent erosional or depositional processes), we can use it as useful tool for paleo sea-level reconstructions (Casalbore et al., 2017). The Ferdinandea depositional terrace has its edge at depths approximating the modern local storm-wave base level, which is defined as the water depth beyond which wave action ceases to stir the sediment bed (Cowell et al., 1999), especially during stormy conditions. Thus, following the model of Casalbore et al. (2017), the Ferdinandea SDT edge was used as analog for deeper terraces located on the other cones of the GVF and formed in the past (but after the LGM), when the sea level was relatively stable and lower than the modern one, with an uncertainty of a few meters (due to the impossibility to distingue the depositional shelf edge from the erosive one, because of lacking of seismic profiles). Within this approach, we assumed that past meteo-marine and oceanographic circulation conditions were similar to the present ones (see **Supplementary Material**) and adopted the post-LGM curve proposed by Lambeck et al. (2011).

Some ROV dives were also carried out (**Figures 2A,B**) by using a ROV PolluxII (400 m depth rated), which allowed the shooting of several high-resolution videos along the slopes of the GVF cones.

RESULTS

Physiography of the Study Area

The GVF is located between 43 and 51 km offshore Sciacca on the western side of a relatively shallow (maximum depth of about 350 m) submarine morphological high, which rises for more than 200 m from the surrounding seafloor (**Figures 1**, **2**). The high covers an area of about 600 km^2 and includes, in addition to the GVF, the Terrible and Nerita banks.

The Nerita Bank is an ellipse-shaped morphological high with a summit depth of −50 m, a nearly 10 km long major axis with a NNE-SSW direction and a 3 km long minor axis. The bathymetric data confirmed the lack of morphological irregularities ascribable to volcanic structures on top of it, as previously indicated by seismic reflection profiles for its subsurface (Civile et al., 2018; Fedorik et al., 2018).

The Terribile Bank is a triangle-shaped submarine plateau with a summit at 28 m water depth. Its top shows a terrace-like morphology, very smooth in the eastern sector, but rugged in the western one, where numerous landslide scars and associated deposits were identified.

The inter-bank areas are characterized by a nearly flat seafloor ranging in depth between 150 and 250 m, occasionally interrupted by fields of circular depressions interpreted as pockmarks related to fluid escape (**Figures 2A,B**). They either occur as isolated features or grouped in WNW to NW-SE oriented clusters. A giant pockmark (300 m large and 65 m deep) was recognized south of the Terribile Bank (**Figures 3A,B**); here, ROV videos (**Figure 3C**) show the very steep walls cutting the seafloor.

Morphological Analysis of the GVF

The GVF is composed of a ten of cones, arranged along a N-S trending belt, nearly 12 km long and 3 km wide (**Figures 2A,B**). The seamounts are distributed on a flat or gently westwardly sloping seafloor, ranging in water depths of 140–250 m. The field is bounded to the west by a NW-SE trending and nearly 100 m high steep scarp, well visible in the southern part of the study area. The volcanic cones are isolated or organized in clusters, which are elongated in a NW-SE preferential direction (**Figure 2A**). Taking into account the spatial separation between the cones (Cañón-Tapia, 2016), all the seamounts were grouped in four clusters (numbered from C1 to C4) (**Figure 2B**). C1 and C3 are composed of isolated cones, while C2 and C4 are composite shoals resulting from the coalescence of two or more simple cones that together make up larger morphological features.

Based on HR multibeam bathymetry data, the seamounts are hereinafter numbered from S1 to S10 and morphologically described in detail moving from south to north.

All the seamounts consist of tephra/tuff cones lacking a summit crater or collapse pit.

C1, the southernmost cluster of the field, is composed of S1, S2, and S3 seamounts lying in water depths of 190–210 m (**Figures 2B**, **4**). S1 and S2 are two flat-topped cones which are very similar to each other with an almost perfect circular shape and very regular and steep slopes (gradient range of 25–26°), without evidence of significant channelized erosive features. S1 has a maximum base diameter of 870 m and a summit located 76 m bsl, while S2 has a base diameter of 1050 m and presents the top at 66 m bsl. Both the tops are constituted by sub-vertical small-scale (about 5 m high) reliefs, similar to plugs or knolls, consisting in the highest part of the volcanic necks highlighted by selective erosion; the plugs are located in the middle of flat or gently sloping (gradient of 6–8°) narrow summit terraces lying between 90 and 100 m water depths. No lava flows were identified along the slopes or around their basis. Their relative proximity (800 m of distance each other) and their very similar morphological features allow us to infer a probable coeval formation, along a nearly N100° oriented eruptive fissure. S3 is a pointy seamount located some 800 m to the north with respect to S2. The summit is located at 105 m bsl while the average basal diameter is about 700 m. It is the only seamount of the field showing an amphitheater-shaped rim around the cone (**Figures 4A,B**); this is 40–55 m high and opened northwestward with, at its base, a 400–600 m large and 20–25 m deep canyon head (**Figures 4A,C**). The canyon runs for nearly 1.5 km in a nearly E-W direction up to the base of the fault scarp bounding westward the volcanic field (**Figures 2A,B**, **4A**); the presence of such a developed channelized feature suggests an intense erosive activity affecting the cone. Finally, numerous isolated blocks, up to 10 m high, likely related to collapse processes, are scattered on the seafloor around C1.

C2 (the Graham Bank, **Figures 2B**, **5**), shows a N130° oriented major axis and is composed of the coalescence of two simple cones, S4 (the remnant of the short-lived "Ferdinandea Island") and S5, which lie on a seafloor between 140 and 180 m bsl (**Figures 5**, **6**). S4 appears as a truncated cone that rises up to 150 m from the surrounding seafloor. It shows an elliptical-shaped base with a N140° direction, and a maximum axis longer than 1.4 km (although it is difficult to exactly measure it due to the coalescence with S5). Its aspect ratio is 0.12 (**Table 1**). The shoal top consists of a sub-vertical volcanic plug, which reaches 9 m bsl (the shallowest point of the whole GVF), being part of a 25 × 10 m elliptical-shaped structure (the knoll), which is elongated in a SW-NE direction. ROV dives carried out on S4 (**Figure 7A**) filmed the knoll abundantly colonized by algae like Sargassum[1] (**Figure 7B**). The knoll (**Figures 5**, **6**) is placed in the middle of a 500 × 380 m elliptical-shaped terrace, which lies between 25 and 30 m water depths. The summit terrace shows a very uneven morphology being characterized by sub-vertical ridges/furrows composed of consolidated pyroclastic material, arranged in a sub-concentric asset and dipping away from the top (**Figures 6**, **7D**); according to Calanchi et al. (1989) they consist of interbedded cinder and ash, with abundant lithic fragments, confirming the explosive activity of the 1831 eruption. Outwardly, a flat or gently sloping (gradient range of 4–8°) seabed occurs, likely corresponding to the top of a depositional terrace, below which the slope sharply steepens. The terrace is up to 70 m large in the NW and SE sectors, narrowing to 30 m in NE and SW ones: its edge lies at water depths of 40–43 m in the N and E sectors, shallowing to 36–38 m in the S and W ones (**Figure 6**). It is likely composed of the black volcanic sediment produced by combined wave/current erosion and wave-driven deposition. The occurrence of sand ripples, imaged by ROV dives (**Figure 7C**), witnesses the active role of waves and currents on the shoal, as

[1]https://storage.googleapis.com/planet4-italy-stateless/2018/11/81b16db4-81b16db4-i-tesori-sommersi-del-canale-di-sicilia.pdf

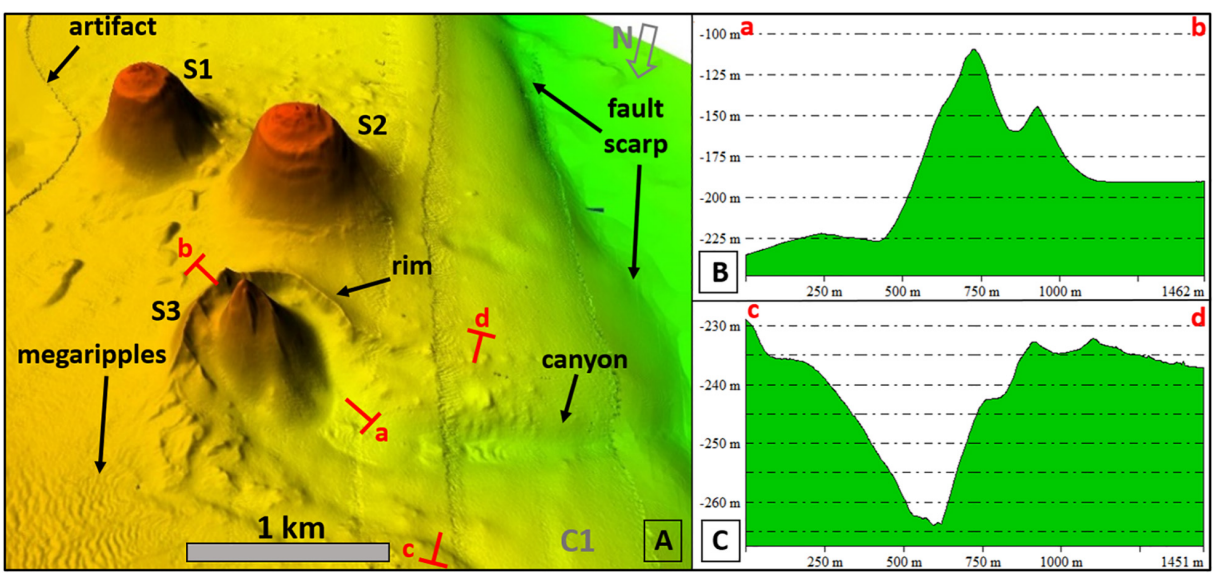

FIGURE 4 | (A) 3D shaded relief image (vertical exaggeration = 4x) of the southernmost cluster of the GVF C1, formed of S1, S2, and S3 seamounts. **(B)** Bathymetric profile (ab) across the pointy-cone S3. **(C)** Bathymetric profile (cd) across the canyon developing from the western base of S3.

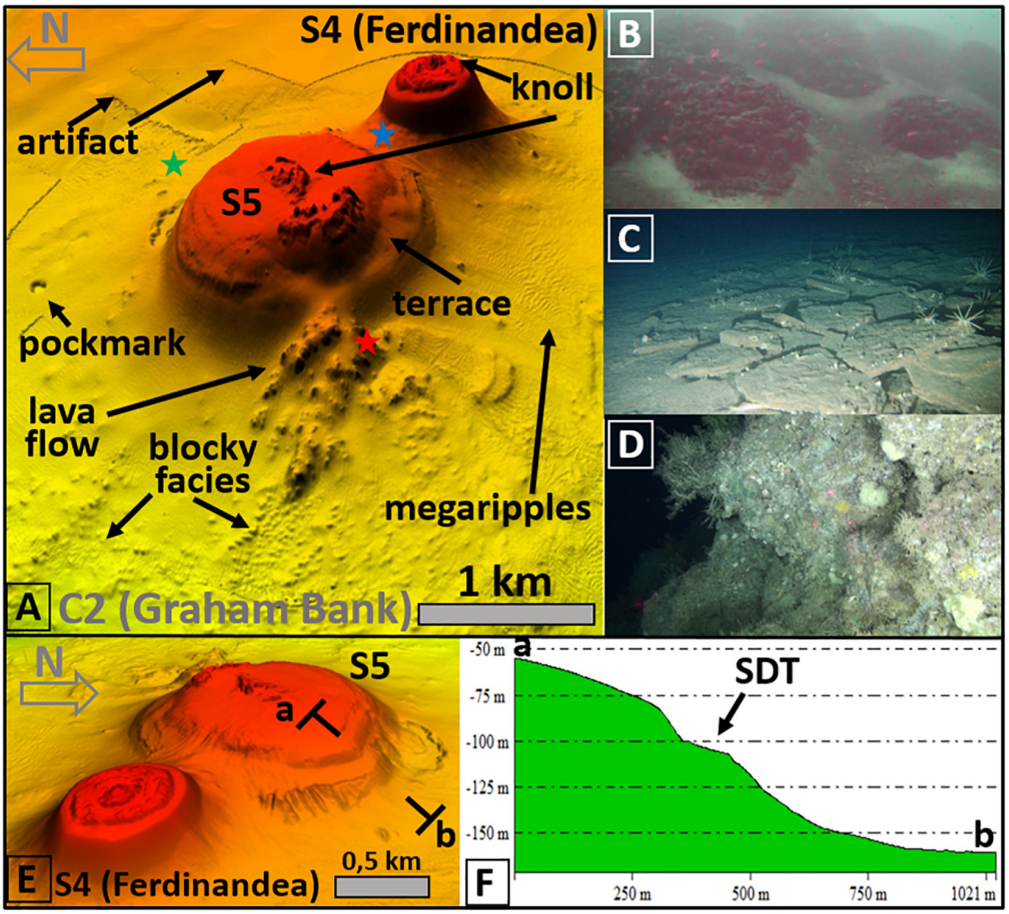

FIGURE 5 | (A) 3D view (vertical exaggeration = 4x) of the Graham Bank (C2 cluster) viewed from the west; the blue star indicates the location a ROV photo **(B)** displaying a group of mounds on the saddle between S4 (the Ferdinandea shoal) and S5 seamounts; the green star indicates the location of the ROV photo **(C)** displaying pieces of semi-consolidated pyroclastic layers on the seabottom; the red star indicates the location of the ROV photo **(D)** displaying the lateral front of a lava flow on the low western side of S5. **(E)** 3D view (vertical exaggeration = 2x) of the Graham Bank from the east showing a 200–300 m wide terrace at about 100 m bsl along the slope of S5, which bathymetric profile (ab) is displayed in **(F)**.

also observed through scuba dives (Colantoni, 1975; Antonioli et al., 1994). The slopes of S4 appear very steep (gradient of 30°, the highest observed in the entire volcanic field, **Table 1**) and regular, without evidence of active erosive process (e.g., gullies or scars), in agreement with its very young age. No lava flows were identified along the slopes or around the base of the cone.

The Ferdinandea cone lies to the SE next of a bigger cone, S5 seamount (**Figures 5A,E**), giving origin to a 200–300 m long and 80–90 m deep saddle among them. On the northern side of the saddle several rounded mounds, up to 5 m high and 10 m large, were observed on both bathymetric data and ROV images (**Figure 5B**). S5, locally called "Secca del Corallo," represents the largest edifice of the field since its circular-shaped base area encompasses some 2.4 km^2 with a maximum basal diameter of 1.8 km (**Table 1**). Its aspect ratio is 0.07, the lowest of the volcanic field. The top (minimum depth of 33 m bsl) is formed by several prominent rocky structures (volcanic plugs/knolls) located in the central and southwestern portions of a nearly flat or gently sloping northwestward terrace lying at 50–60 m water depths. At 100–115 m water depths, the cone shows a break in slope associated with another terrace, which is more developed (200–300 m wide) on the southeastern side of the edifice (**Figures 5A,E,F**). The slopes exhibit abundant evidence of erosive activity proving an older age with respect to the Ferdinandea cone. In fact, the lowest part of the eastern flank is cut by several gullies, up to 150 m long and 6 m deep, which are indicative of slope failures and sediment transport into deeper water in form of debris flows or turbidity currents. The northeastern flank and its base are characterized by a few scars, up to 5 m deep (**Figures 5A,E**), likely enhanced by hydrothermal activity of a fumarole field, whose presence is confirmed by gas bubbles recorded by multibeam sonar echos in the water column (Falzone et al., 2009) and by ROV images and gas samples (Coltelli et al., 2016). Here, ROV images show the presence on the seabottom of few cm thick sharp-cornered plates of consolidated pyroclastic sediment (**Figure 5C**). The seafloor at the base of the western flank shows an irregular morphology due to the presence of a 1 km long and 1 km wide fan-shaped lava field,

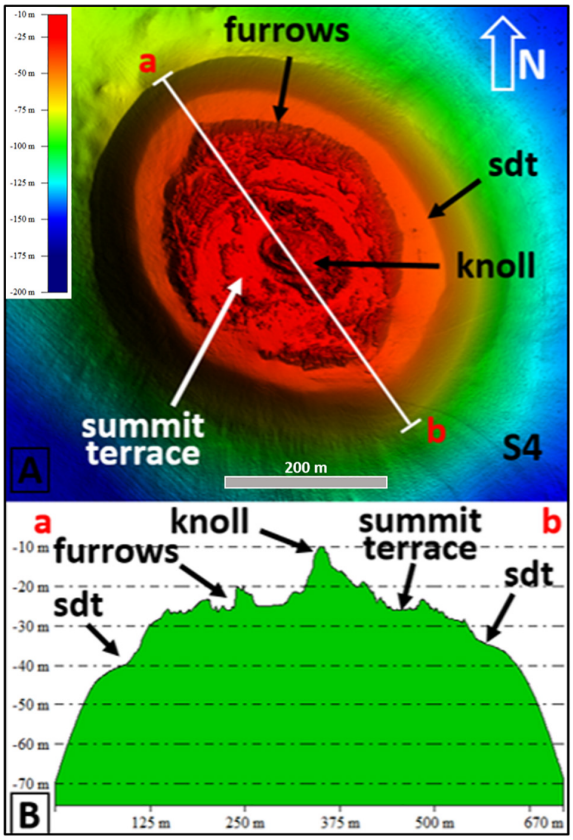

FIGURE 6 | (A) Very high-resolution shaded relief image of S4 shoal (Ferdinandea volcano), with a NW-SE topographic profile **(B)** well imaging the knoll, furrows, summit terrace and submarine depositional terrace (SDT); the SDT's edge shallows from NW to SE.

the only one well-recognized in all the mapped area, composed of three or four different blocky-lava flow units (**Figures 5A,D**). The southernmost portion of the lava field shows a smoothed morphology likely due to the partial covering by both the eroded material of the cone flanks and pyroclastic fallout deposit erupted by the adjacent Ferdinandea cone in 1831. Westwards, a blocky facies extends for more than 1 km from the front of the lava flow, partially buried by sediments. A field of megaripples (up to 2 m high) occurs in water depths between 160 and 200 m, on the southern side of C2 (**Figure 5A**), witnessing an intense reworking activity. Finally, a pockmark is located to the north of the Graham Bank showing a width of 100 m and a depth of 7 m (**Figure 5A**).

C3 is composed of S6 and S7, two isolated pointy seamounts, located 3 and 4.5 km northwards from the Graham Bank, respectively (**Figures 2B**, **8A**). The tops lie at 122 and 98 m bsl while the average basal diameters are 730 and 870 m large, respectively (**Table 1**). S6 is 118 m high and shows an almost perfect circular basal shape. S7, locally called "Secchitella" ("small shoal" in Italian), has a NW-SE trending elliptical-shaped base. Both the seamounts show several important evidence of mass wasting processes, confirmed by hundred-meter-wide scars along the slopes and hummocky morphologies at their bases. In particular, the seafloor around S7 is covered by a blocky facies of boulder deposits extending up to 700 m far from the southeastern side of the cone.

C4, locally called "Bancazzo," is the northernmost cluster of the field (**Figure 8B**), being located only 44 km offshore Sciacca. It is composed of at least three coalescent truncated cones (S8–S10), aligned along a NW-SE direction. The shape of the three seamounts is irregular with basal diameters ranging from 1000 to 1350 m (**Table 1**), although an accurate estimation is difficult due to their partial overlying. The summit depth ranges from 75 m for S9 to 83 m for both S8 and S10; it was measured at the prominent knolls, lying in the middle of the top platforms at around 85 and 90 m, for S9 and S8–S10, respectively. On the northern side of S8 a small cone with a summit at −82 m is observed, together with another one between it and S9, as belonging to the same edifice (see also Civile et al., 2018). The seabottom around C4 shows a rugged morphology due to the presence of deposits of boulders (up to 200 m large), which are spread up to 1 km far from the cones.

Morphological Analysis of the Terribile Bank

The southwestern side of the Terribile Bank displays an overall step arrangement with three, NW-SE oriented main scarps, up to 20 m high, and four terraces, whose edge lies at about 130, 105–110, 85–90, and 60 m bsl (**Figures 2A,C,D**). Based on the depth of its inner margin the deepest terrace might be related to the sea level reached during the LGM, even if the lack of seismic reflection images limits the reliability of our interpretation. It almost continuously bounds the whole Terribile Bank (slightly shallowing from NW to SE, likely due to tectonic tilting produced by the proximity to the fault on the eastern side of the bank, see Ferranti et al., 2019). Similar features were recognized on the Anfitrite Bank at 120–130 m bsl and associated with the LGM paleo-coastal cliff by Civile et al. (2015) on the basis of seismic reflection profiles. The shallowest step lying at 65–85 m bsl was interpreted by Civile et al. (2018) as a NW trending currently active normal fault developed during late Miocene and later reactivated by the transpressive tectonics affecting the Terribile and Nerita Bank, although a correlation with a paleo-coastal cliff related to younger stillstands during the last sea-level rise (e.g., Younger Dryas stadial) could not be ruled out (see Zecchin et al., 2015).

On top of the Terribile Bank, a field of numerous (ca 30) flattened truncated cones, isolated or clustered, sometimes coalescent, are spread over a 25 km^2 wide area ranging in depth from 100 to 40 m bsl (**Figures 2A,C,E**), giving origin to the TVF. Few of these cones were also identified in previous studies (i.e., Falzone et al., 2009; Coltelli et al., 2016; Civile et al., 2018; Lodolo et al., 2019b), while most of them are recognized for the first time in this work. Although the lack of high-resolution bathymetric data does not allow a detailed morphological analysis of the TVF, generally the cones show a smaller size in comparison with those of the GVF; indeed their width ranges between 100 and 300 m, while height from 10 to 50 m. The cones have a circular or elliptical (with maximum axis showing a predominant NW-SE

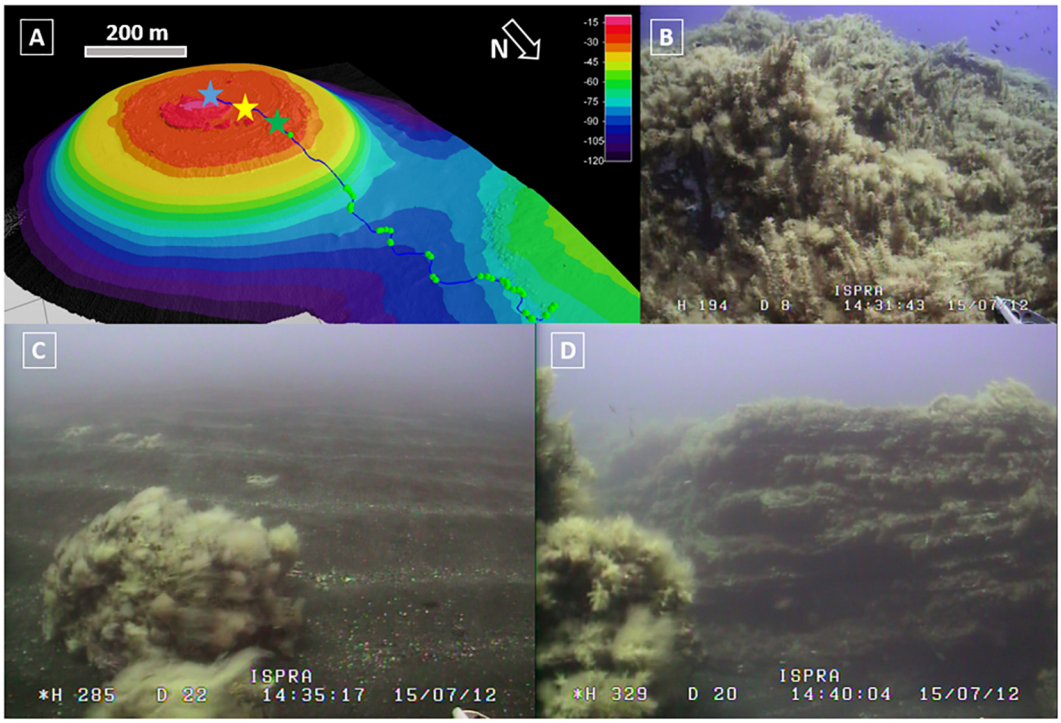

FIGURE 7 | (A) ROV dive on top of the Ferdinandea shoal (S4). The blue star indicates the location of **(B)** showing the volcanic knoll, which represents the shallowest point (−9 m) of the whole field, completely colonized by gorgonians. The yellow star points to the location of **(C)** displaying the seafloor of the summit terrace characterized by black sand ripples. Finally, the green star indicates the location of **(D)** where the furrows are imaged.

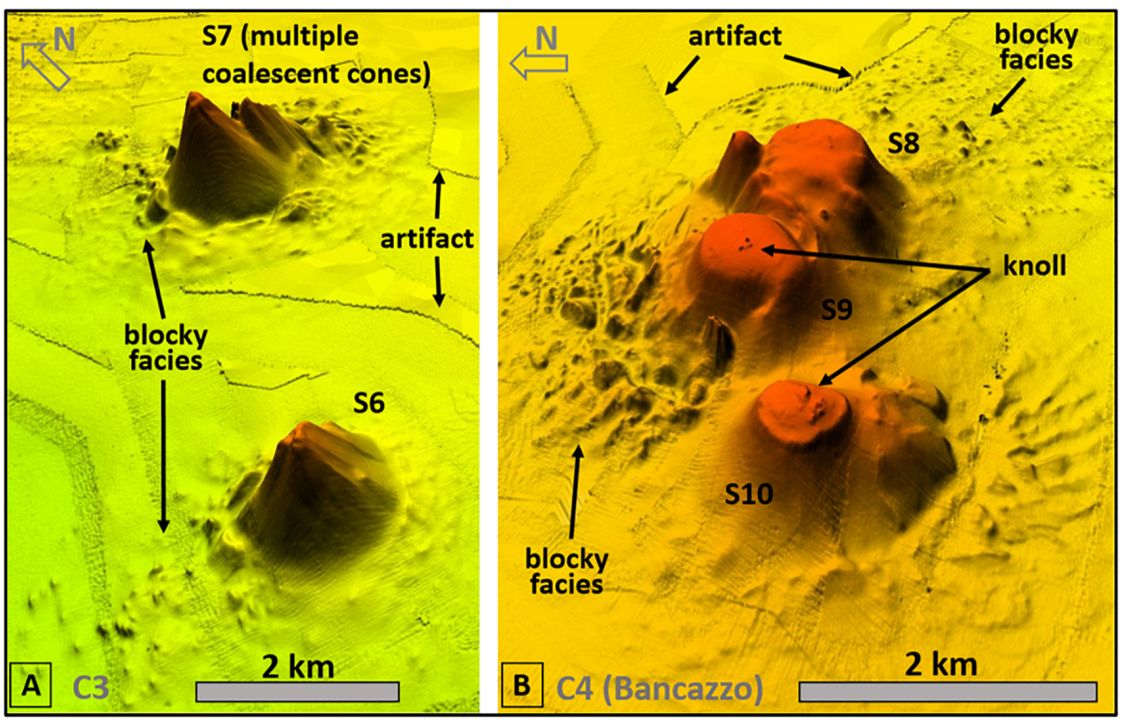

FIGURE 8 | 3D view (vertical exaggeration = 4x) of **(A)** C3 Cluster – **(B)** C4 cluster (Bancazzo).

direction) basal shape. Summit depth ranges from 28 to 100 m bsl. The great part of the cones is flat-topped with summit terraces between 40 and 80 m water depths.

DISCUSSION

Morphological Evolution of the Seamounts and Relationship With Underwater Volcanic Processes

The seamounts of the GVF show heights from 88 to 144 m, maxima basal diameters ranging from 750 to 1850 m and planimetric basal areas from 0.42 to 2.40 km^2, with a median value of 0.8 km^2 (**Table 1**). The depth of their summits varies between 9 and 122 m. They have steep flanks, with gradients ranging between 18 and 29°, except for the Ferdinandea cone (S4), which shows steeper flanks being the youngest and best-preserved volcanic edifice of the field. The occurrence of such steep gradients, together with the non-cohesive nature of the sediments, explains the numerous slope failures identified within the volcanic field. The cone slopes show abundant evidence of widespread flank failures suggesting a long-lasting and intense erosive activity (e.g., C3 and C4 clusters); this process is confirmed by the rugged seabottom at their bases highlighted by blocky deposits, which were transported gravitationally downwards. Instability triggering processes may include syn-eruptive shaking and volcano-tectonic activity as well as cyclic loading due to storm-waves.

The aspect ratio (H/W) of the cones ranges between 0.07 and 0.16, with a median value of 0.13, which is within the range (0.1–0.3) reported for other submarine cones worldwide (e.g., Romero Ruiz et al., 2000; Stretch et al., 2006; Tempera et al., 2013). The estimated volume ranges from 0.018 to 0.169 km^3 with a median value of 0.051 km^3, which is a little smaller than that reported for other monogenetic volcanic field (e.g., Romero Ruiz et al., 2000). This value confirms the relative low amount of lava erupted during underwater monogenetic eruptions. Correlations were observed between maximum and minimum diameters and between height and average basal diameter; seamount height increases with increasing of minimum basal diameter, as well as volume with basal surface and with average basal diameter, as expected. A general increase in volume with increasing height was also observed. The lack of linear relationships between some other morphometric parameters (i.e., between water depth and cone height) suggests that the cones did not develop in a simple self-similar way (Stretch et al., 2006).

The GVF cones likely grew in shallow water and thus are related to Surtseyan-type eruptions. The lack of summit craters on the pointy cones indicates a low explosivity due to the significant water load, allowing to discriminate the very shallow water eruptions (Surtseyan-type) from the deeper ones (submarine-type) (Kokelaar, 1983, 1986; Cas and Giordano, 2014).

Some seamounts are isolated, whilst others form coalescent cones. Although the occurrence of multiple cones could be interpreted as due to polygenetic activities, we infer that it is due to cones superimposition related to the same eruption, where different vents interfere with each other (as evidenced by Corazzato and Tibaldi, 2006 in subaerial environment). This inference is based on several evaluations on the cone features, which are discussed in the following. The ellipticity of the S7's base, could be explained as due to syn-eruption sector collapses affecting the eastern flank of the cone or alternatively as the result of the coalescence of two or three volcanic vents (see Tibaldi, 1995); this latter interpretation entails the need of a NW-SE oriented fissure. Similarly, the presence of the amphitheater-shaped rim around S3 could be interpreted as the combined effect of a syn-eruption slope failure and bottom-current erosion, instead of a secondary intra-crater activity (**Figure 4A**). The particularly similar morphology (i.e., size, slope gradient, level of erosive dismantlement) between cones located at relative short distance each other (i.e., S1–S2 seamounts and those forming the C4 cluster), together with the comparable depth of their summit terraces, could be explained as generated during the same eruption along nearly WNW-ESE trending volcanic fissures. The lack of morphological evidence for such fissures connecting the cones could be ascribed to pyroclastic/epiclastic deposits, produced during the explosive activity and/or transported by erosive-depositional waves-currents processes mantling them. Lineaments of isolated cones may be due to the rapid cooling of the eruptive fissure during the same eruption, favoring the progressive blocking of magma ascent through the entire dyke and leading to the emission of lava from separate vents along the same feeder dyke (see Bruce and Huppert, 1989; Head et al., 1996). This process is enhanced in submarine environment due to the very high heat conduction through water.

All these considerations confirm the monogenetic nature of the GVF seamounts. In this condition, according to Coltelli et al. (2016), the extremely regular morphology of the Ferdinandea slopes and the lack of any secondary crater, fissure or simple volcanic vent, allowed us to rule out the occurrence of any other eruptive activity after the 1831 eruption, in contrast with some chronicles that reported new volcanic activities in 1833 and 1863 on the same cone (Antonioli et al., 1994; Falzone et al., 2009).

Within the GVF some cones show a pointy shape, whereas others exhibit a terraced top. With the exception of the shoals composing the C2 cluster, the depth of the terraces of the flat-topped cones ranges between 80 and 100 m. Generally, morphometric parameters (height, H/W ratio, and basal diameter ratio) of flat-topped cones show correlations with depth (e.g., Clague et al., 2000a; Mitchell et al., 2012b; Casalbore et al., 2015), suggesting that the latter plays an important role in their formation. Although the wave erosion is the predominant process responsible for modeling flat-topped cones, other factors come into play: (1) lava infillings of summit craters or calderas (Clague et al., 2000b); (2) long-lasting overflowing submarine lava ponds (Clague et al., 2000a); (3) high effusive rates associated with areas of high magma supply (McClinton et al., 2013); (4) the combined effect of forced spreading of the eruptive submarine plume upon reaching the water-air density barrier and wave erosion (Mitchell et al., 2012b; Casalbore et al., 2015).

The seamounts recognized within the GVF and in other shallow-water submarine areas worldwide, such as

the Syrtlingur, Jólnir and Surtla satellite shoals of Surtsey (Kokelaar and Durant, 1983; Romagnoli and Jakobsson, 2015), consist of spatter/tuff cones, typical of the Surtseyan-type eruptions. The large amount of scarcely cohesive pyroclastic material forming the cones could have been easily eroded by wave action during Late-Quaternary sea-level change, leading to the formation of summit planar surfaces. The summit of the flat-topped seamounts composing the GVF is often characterized by sub-concentric furrows and ridges (see for example the Ferdinandea shoal, **Figures 5**–**7**), as also observed at Surtla (Kokelaar and Durant, 1983), or at the Princess Alice Bank and Terceira (Azores, Casalbore et al., 2015; Mitchell et al., 2016), where these features are likely the result of differential erosion of the coarse-fine and/or more-less consolidated volcanic strata. Selective erosion of individual pyroclastic layers with varying resistance may leave the concentric furrows and ridges (Mitchell et al., 2016). Similarly, the knolls, often found on the cone summits, represent the remnants of the conduit supplying the volcanic vent exposed by selective erosion. Analogously to those identified on the tops of Surtsey' satellite shoals (Jakobsson et al., 2009), knolls rise vertically to heights of 5–15 m above the surroundings with a diameter of about 20–50 m. These structures represent semi-consolidated spatter deposits, which have undergone palagonitization near the volcanic vent; the high temperature led to palagonite-tuff formation to a higher level than elsewhere (Norrman and Erlingsson, 1992; Jakobsson et al., 2009).

Distribution of Volcanic Seamounts and Tectonic Control

The GVF and TVF volcanic fields, identified offshore southwestern Sicily, prove the repeated occurrence of a monogenetic volcanism, which is part of a wider and scattered one affecting the northwestern Sicily Channel since the Upper Miocene (Calanchi et al., 1989, among others). This volcanism represents a peculiarity since it took place within a tectonic transpressive transfer zone associated with a continental rifting, outside of the typical geodynamic settings of other volcanic fields such as subduction or oceanic rift zones, and far from long-lived volcanic systems.

The distribution and shape of seamounts within the volcanic fields, as well as the orientation of the main axis of the cluster in which they are grouped, provide important insights into the interaction between volcanism and tectonics in the formation of the fields, since tectonic structures furnish a preferential pathway for magma ascent. Indeed, the alignment of pyroclastic cones and vents as well as the elongation of cone base are generally related to the magma-feeding plane, and the strike of the latter is in turn strongly influenced by the main tectonic stress axis (Tibaldi, 1995). A similar interaction was observed in other submarine volcanic areas, such as offshore the Azores (Casalbore et al., 2015) and Canary islands (Romero Ruiz et al., 2000).

The cones of the GVF are generally grouped into clusters or merged to form coalesced edifices, both aligned along NW-SE to WNW-ESE preferential directions (**Figure 9A**). The base of the cones varies from circular- to elliptical-shaped. Although the distribution of both syn- and post-eruptive deposits on the slopes of the cones down to their bases is considerably influenced by the main currents direction, it also strongly depends on the shape and strike of the volcanic conduit/feeder dykes. Thus, the ellipticity of the volcanic cones reflects the orientation of preferential tectonic stress axis controlling their emplacement. The elliptical cones of the GVF have their main axes preferentially aligned NW-SE (**Figure 9B**). The interaction between volcanism and NW-SE tectonic structures in controlling

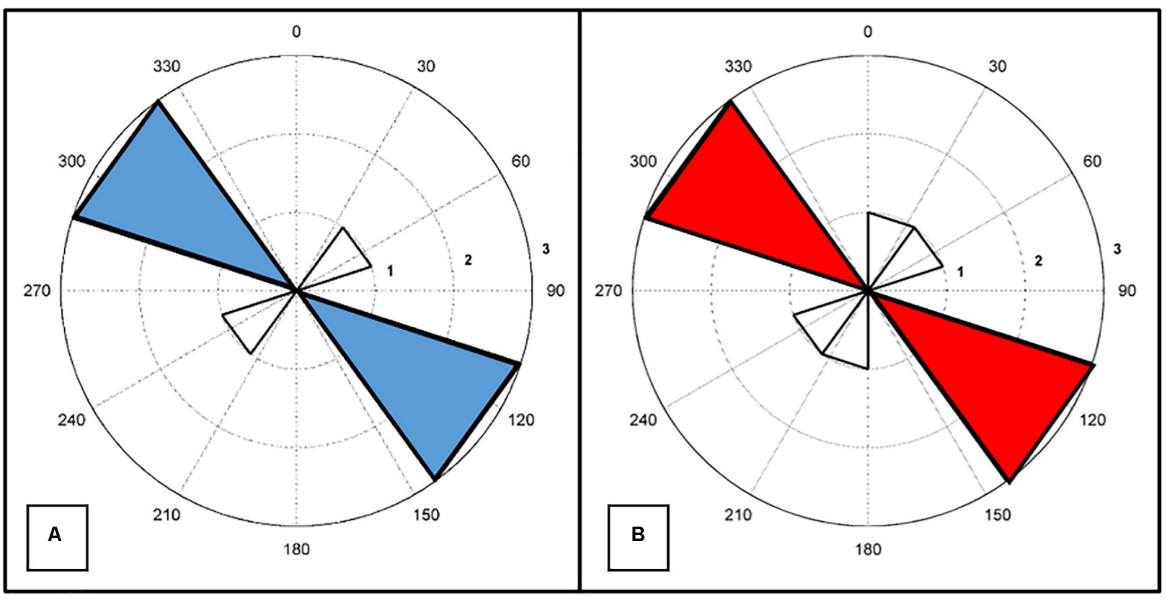

FIGURE 9 | Rose diagrams related to the trend of maximum elongation axis of the clusters of cones **(A)** and cone bases **(B)**.

the distribution and shape of the volcanic cones is also confirmed by the maximum axis direction of some elliptical-shaped cones forming the TVF. Finally, the role of the NW-SE preferential structural direction is corroborated by the alignment of three other volcanic centers (Tetide, Anfitrite, and Galatea) located on the adjacent Adventure Plateau (**Figure 1**) and by the alignments of several pockmarks observed within the study area (**Figure 2**) and to the west of the GVF (Spatola et al., 2018). Some of the above-discussed pockmarks could be also responsible for the recent strong gas releases observed within the area and may have been inaccurately associated with the repeated volcanic activities of the last few centuries reported by several authors (Antonioli et al., 1994; Guidoboni et al., 2002; Bottari et al., 2009; Falzone et al., 2009). The NW-SE direction is associated with the Pliocene-Quaternary continental rift-related processes that generated the three NW-SE oriented and fault-controlled grabens of Pantelleria, Malta and Linosa, characterizing the central part of Sicily Channel.

The overall N-S alignment of the GVF cones, together with the other volcanic centers identified south (i.e., Cimotoe volcano, Calanchi et al., 1989; Civile et al., 2015) and north (a few small isolated cones, Civile et al., 2015, 2018; Lodolo et al., 2019a) of the field, reflects the orientation of the Capo Granitola-Sciacca Fault Zone (Fedorik et al., 2018; **Figure 1**). Based on seismicity data, Calò and Parisi (2014) interpreted this transfer zone as the shallow expression of a sub-vertical lithospheric shear zone favoring magma ascent in this region.

Thus, two main tectonic systems, N-S and NW–SE trending, consistent with the main regional tectonic lineaments affecting the Sicily Channel, seem to control the arrangement of the volcanic fields and the other volcanic centers of the surrounding area (as also inferred by Civile et al., 2018; Spatola et al., 2018; Lodolo et al., 2019a,b). These two preferential orientations are also confirmed by the occurrence of magnetic (Colantoni et al., 1975; Lodolo et al., 2012) and gravity (Civile et al., 2008; Lodolo et al., 2019b) anomalies.

Relationship With Sea-Level Change

Wave erosion is very efficient in shoaling volcanic islands and flattening their summits, especially if made of poorly consolidated materials such as those built by Surtseyan-type eruptions. The flattening process is more efficient for volcanic cones without topping lava flows, which may represent a resistant cap protecting the island from wave erosion (Schmidt and Schmincke, 2002). On the other hand, erosive processes will slow considerably once the much more resistant volcano interior, composed of the feeder dyke and palagonite tuff, is reached (Jakobsson et al., 2000). Together with surface waves, the intensity and recurrence of extreme-wave events, like storms and even tsunamis, should have a very high impact in both flattening the tops of volcanic shoal, and creating SDTs along their slopes. In fact, strong storms and tsunamis constitute high-energy and low-frequency events that cause extensive erosion, sediment transport and deposition in a very short time and over large areas (Paris et al., 2009).

Wave-induced shear stresses and currents on the bottom are efficient down to considerable depths, at least down to storm-wave base (Cas et al., 1989; Ramalho et al., 2013), creating shallow marine abrasion surfaces (White, 1996; Schmidt and Schmincke, 2002). The depth to which the top platform is abraded is the result of the interplay of different factors and processes, including depth of sea level at the time of eruption, vertical movements due to volcano-tectonic deformation, sediment compaction, wave/current energy, time and direction of exposure to wave/current attack, rock resistance, lava and sediment progradation, coral reef growth and biogenic production (Quartau et al., 2010; Ramalho et al., 2013). Sea-level oscillations significantly influence the depth to which the top wave-cut platform is abraded; this depth represents the local wave base level (Ramalho et al., 2013).

Following the models by Cas et al. (1989) and Corcoran and Moore (2008), relative to the post-eruptive degradational phase of monogenetic shallow marine volcanoes, a wave-planned top is developed on the submarine volcanic edifice becoming gradually stable and colonized. Wave and current activity, together with periodic storms, sweep material off the platform, spreading over its edge the eroded debris, which is re-deposited along the slopes of the cone and down there; steep progradational wedges are thus formed at the edge of the platform, causing its gradual enlargement (Romagnoli and Jakobsson, 2015).

"Ferdinandea Island" is a well-documented example of the post-eruptive transitional stage from volcanic island to shoal. Since its formation, destructive forces have been active for almost 200 years, during which the cone has suffered rapid and severe subaerial and submarine erosion due to strong wave and current activity causing significant modification of its original size and shape: i.e., a reduction from nearly 210 to 140 m of height from the seabottom and an enlargement of its basal surface. Scuba (Colantoni et al., 1975; Antonioli et al., 1994) and ROV dives (this work, **Figure 7**) revealed that the flat seafloor of the summit terrace between the volcanic plugs (25–28 m bsl), is made up of black coarse loose tephra organized in sand waves. A similar sedimentary facies characterizes the top of the underlying SDT, whose edge lies between 36 and 43 m (corresponding to the local storm wave base-level), suggesting that wave and current erosion is still quite strong at that depth. The morphological asset of the Ferdinandea's SDT reflects the distribution of wave force since its edge shallows from NNW to SSE (**Figure 6**) in agreement with the prevailing wave direction, which is toward ESE, being strongly influenced by the northwesterly winds (Arena et al., 2015, **Supplementary Material** and **Figure 2** therein).

The summit of the Ferdinandea cone was eroded down to −28 m over nearly 200 years following its eruption. The bathymetric surveys carried out by IIM from 1890 to 2014 (Sinapi et al., 2016) allow us to document a faster erosive rate during the first 50–60 years (**Figure 10**), as expected. This has been also observed at the satellite centers of Surtsey, Surtla, Syrtlingur and Jólnir (**Figure 10**), which represent excellent modern analogs for understanding the post-eruptive phase of the Ferdinandea shoal and others cones of the GVF. Syrtlingur and Jólnir reached a maximum height of 70 m asl at the end of the 1963–67 eruption, while Surtla only approached the sea surface; a few weeks after

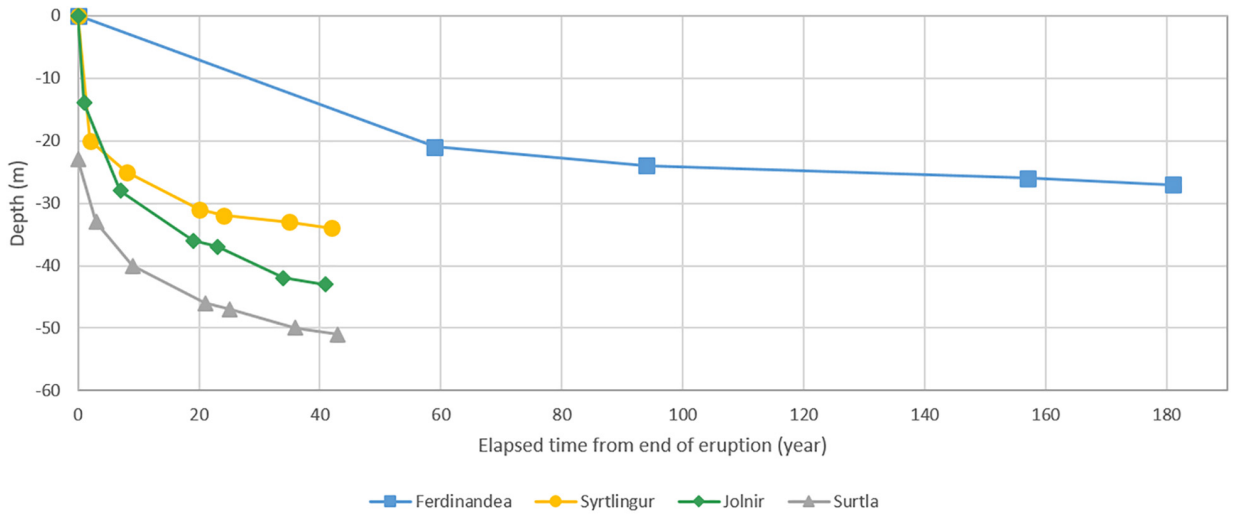

FIGURE 10 | Graph of depth with time of the average depth of the flat summit of Surtla, Jólnir, and Syrtlingur until 2007 (Jakobsson et al., 2009) and Ferdinandea until 2012. The efficacy of wave-current erosion rapidly decreases with increasing depth.

the eruption ceased they were washed away by wave action (Romagnoli and Jakobsson, 2015). Successively, the shoals were further abraded by the sea, producing summit platforms, which were gradually enlarged and lowered (Jakobsson et al., 2009) as the result of the reworking of volcaniclastic sediments due to erosion by waves and bottom currents. In 2007, the measured depths of the Surtla, Jólnir and Syrtlingur top terraces were 51, 43, and 34 m, respectively (Romagnoli and Jakobsson, 2015). In particular, the summit of Surtla was eroded down to 45 m depth over nearly 18 years following its eruption (Kokelaar and Durant, 1983) and down to 51 m depth over the next 26 years (**Figure 10**), suggesting that the wave erosion depth level is deeper here, if correlated to the more energetic wave climate of North Atlantic Ocean with respect to the Sicily Channel (see **Supplementary Material**).

A similar process occurred at the Baixa da Serreta Bank (offshore Terceira Island, Azores), the probable site of the 1867 submarine eruption (Weston, 1964), where the planar surface identified in 2011 at −30/−40 m was interpreted as the result of wave erosion of scarcely cohesive volcanic products (Quartau et al., 2014).

On the basis of the present-day maximum depth of the summit abrasion terrace (28 m bsl) of the Ferdinandea shoal, which has to be considered still under development, and taking into account the trend of its erosive rate (**Figure 10**), the local wave base level can be reasonably placed at least at 30 m bsl. Considering the differences in the respective wave climates (see **Supplementary Material**), this value is lower than that observed in Atlantic Ocean, where the Surtsey's volcanic satellites and Baixa da Serreta Bank are placed, but higher than the value relative to the Mediterranean. This latter assumption is based on two evidence: (1) the wave climate of the study area is more energetic than the average climate of the Mediterranean (Drago et al., 2010; Arena et al., 2015; **Supplementary Material**); (2) the value of the local storm wave base-level, estimated between 36 and 43 m bsl on the basis of the depth of Ferdinandea SDT depositional edge (or rollover depth) (**Figure 6**), is higher than that calculated in other areas of the Mediterranean, e.g., 20 ± 10 m bsl in the Tyrrhenian Sea, Casalbore et al., 2017; 20–25 m bsl Hernàndez-Molina et al., 2000 and 32 m bsl, Mitchell et al., 2012a in western Mediterranean. Moreover, it is worth noting that these latter values are referred to a costal environment, while the GVF cones are shoals and thus the erosion affecting them is to be considered omnidirectional.

Based on seismic reflection profiles, Ferranti et al. (2019) estimated a relatively moderate growth rate of 0.2 mm/yr during the Plio-Quaternary for the southern segments of the CGFS and SFS, along which the GVF and Terribile bank are respectively aligned. This rate is also confirmed by GPS data of the Campobello di Mazara station (about 10 km NW of Capo Granitola, **Figure 1**), which recorded an uplift rate of 0.2 mm/yr between 2009 and 2015 (Valentina Bruno personal communication). As above discussed, based on the depth of its inner edge (130 m bsl), the flat terraced surface, identified at the base of the SW portion of the Terribile Bank (**Figures 2A,D**), may be related to the sea-level reached during the LGM (19–20 ka B.P. when sea level was −125 ± 5 m below the modern one, Fleming et al., 1998; Siddall et al., 2003; Clark et al., 2009), by considering an overall tectonic uplift of nearly 4 m over the last 20 ka. Moreover, such a small uplift is to be considered within the level of uncertainty related to the estimation of LGM sea level. These data suggest the lack of significant tectonic variations affecting the study area in the last 20 ka. The compaction of the tephra deposits through time may have contributed, even if in a small proportion, to lower the Ferdinandea shoal and thus to increase the depth of its summit terrace. Surtsey Island could represent a good analog, since a series of GPS surveys were carried out during the years following its recent formation. Surtsey was affected by a general subsidence (including the crustal sagging due to the load of the erupted material and

possible compaction of the seabed sediments) of about 1.0–1.5 m during the 35 years following the end of the eruption, with a rate decreasing from 15–20 cm/yr for 1967–1968, to 1 cm/yr for 1992–2000 and finally to 0.5 cm/yr for 2000–2002 (Moore et al., 1992; Sturkell et al., 2009). Although Surtsey and GVF lie in different geodynamic settings, we can reasonably apply this subsidence rate to the Ferdinandea cone; moreover, this rate is probably overestimated for the Ferdinandea case, because of its lower load in comparison with that of Surtsey, having the two volcanic centers different size and stratigraphy (succession of lava flows and pyroclastic units vs. pyroclastic material). Thus, the Ferdinandea subsidence associated with compaction could be estimated in less than 1 m since its formation, and thus its contribution in lowering its summit as well as the other cones of the GVF considered negligible.

On the basis of the above considerations and assuming uniform rates for the tectonic uplift during the post-LGM, we can reasonably discount the minimum contribution of tectonic deformations and subsidence affecting the GVF; moreover, these processes compensate each other and their values could be considered within the level of uncertainty related to precisely measure the depth of the summit terrace of the Ferdinandea volcanic cone. Moreover, the deformation induced by volcanic processes (i.e., inflation-deflaction) for scattered small monogenetic volcanic cones, as the case of those forming the GVF, is highly attenuated because of the lack of any plumbing system, magmatic reservoir, etc., and thus considered negligible as well.

Consequently, any submarine structure shallower than ca. −155 m (125 ± 5 = depth of LGM + 30 ± 5 m = depth of the wave erosion depth) below present sea level was potentially affected by wave erosion during the LGM, if created before the LGM. Therefore, following the model proposed by Mitchell et al. (2012b) and taking into account the Global mean sea level curve for the study area (Lambeck et al., 2011), the cones with a top shallower than ca −155 m and lacking a flat summit surface typical of a wave-eroded platform (i.e., S3, S6, and S7 seamounts, **Table 1**) have survived erosion during the LGM; otherwise, they should have been flattened during the LGM. Thus, they are likely younger than the LGM (**Figure 11**).

S1, S2, S8, S9, and S10 seamounts show summit terraces, at around 90–100 m water depths. Thus, they were likely eroded during the transgressive phase following the LGM (**Figure 11**). Taking into account the analogy with the wave erosion depth of Ferdinandea shoal (–30 m), we can reasonably hypothesize that they were mostly eroded when sea level was at least −60/−70 m below present sea level and thus during the interstadial stillstand of the Younger Dryas (YD), a geologically short period of cold climatic conditions, which occurred between 12.8 and 11.5 ka (Muscheler et al., 2008), when sea level was 60–65 m below the present level. This stadial would have favored the development of restricted abrasion platforms in several regions worldwide (see Salzmann et al., 2013; Green et al., 2014, among others) including the Sicily Channel (Civile et al., 2015; Zecchin et al., 2015), like that recognized at about 60 m bsl on the Terribile Bank (**Figures 2A,C,D**). Civile et al. (2015) recognized along the flanks of several sedimentary banks of the Sicily Channel (e.g., Pantelleria Vecchia) a relatively flat surface between 60 and 75 m water depths connecting two scarps, that might have formed during episodes of rapid relative sea level rise (i.e., Melt-Water Pulse MWP-1A and MWP-1B, Liu and Milliman, 2004), following the cliff overstep' transgressive model by Zecchin et al. (2011).

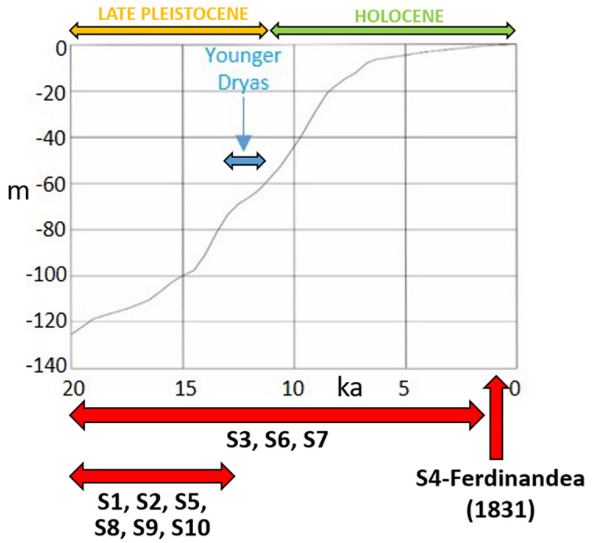

FIGURE 11 | Correlation between mean sea level curve referred to the study area (Lambeck et al., 2011) and proposed possible ages of the volcanism generating the cones of the GVF; see the text for further details.

The summit terrace of S5 shallows from NW to SE, confirming the relationship with the main NW-SE oriented wave provenance (Arena et al., 2015; **Supplementary Material** and **Figure 2** therein) as also observed on the Ferdinandea's SDT. The lowest values of slope gradient and aspect ratio of the GVF (**Table 1**) reveal an ancient age; this is also confirmed by the morphological asset of S5, which suggests that it suffered a longer-lasting severe erosion (probably amplified by the presence of a large amount of pyroclastic material) in comparison with the other cones of the field. Its summit terrace lies between 50 and 60 m of depth suggesting that S5 was flattened during the sea level rise of the current Holocene interstadial. Moreover, S5 shows a restricted depositional terrace, which is well-developed on the southeastern sector of the cone (**Figure 5**); its outer edge lies at about 100–110 m water depths. Consequently, by applying the storm-wave base level relative to the Ferdinandea shoal (36–43 m bsl) to the S5, we can hypothesize (taking into account that the lack of seismic reflection profiles limits the reliability of our interpretation of these marine terraces) that its SDT likely formed when sea level was about 60–70 m lower than the modern one, and thus during the YD. Therefore, we speculate that S5 may have erupted after the LGM, giving origin to a nearly 1 km large island. Successively, it was partially eroded during the YD (when the middle-slope SDT formed) and finally was flattened during rising sea level following the YD, more precisely between 6 and 8 ka, when the sea level was nearly 20 m below present sea level (**Figure 11**).

Among all seamounts of the GVF, S5 cone is clearly oversize (3 times larger in volume than the Ferdinandea shoal and

at least 5 times larger than the average value of the other cones, **Table 1**). Taking into account that the S5 eruption likely occurred in shallower water with respect to the 1831 Ferdinandea eruption, and, consequently, it was subjected to a significantly minor hydrostatic pressure, a stronger Surtseyan-type activity (Kokelaar, 1983, 1986; White, 1996) could justify such a larger volume in comparison with those of the other cones of the field.

On the basis of the above-described analysis, we can reasonably hypothesize a post-LGM age for the monogenetic submarine volcanism forming the GVF (**Figure 11**), without any clear migrating pattern with age.

Moreover, paleontological analysis of faunal elements associated with sub-fossil coral deposits found between C3 and C4, indicated a post-LGM emplacement (Di Geronimo et al., 1993); while radiocarbon dating of these corals span the last 10 ka, indicating that they were accumulated during the Holocene (Lodolo et al., 2017). The latter authors associated the origin of the coral deposit to periodic slope failures, possibly triggered by volcanic and/or seismo-volcanic activity (like that reported during Ferdinandea eruption; Gemmellaro, 1831), dislodging corals (dead or alive) from the steep flanks of volcanoes on which they lived, hypothesizing the occurrence of an active volcanism in the area during the last 10 ka.

Finally, as regards the Terrible volcanic field, it includes at least 30 small (height from 10 to 50 m) truncated and multiple coalescent cones. Most of them likely consist of the volcanic necks or the hard volcano-interiors representing the remnants of severely eroded volcanic edifices. This suggests that a likely older submarine volcanism affected this area before migrating westward to create the GVF. Although the lack of high-resolution bathymetric data does not allow a detailed morphological analysis of these cones, many of them show a summit terrace between 40 and 80 m water depths, suggesting that they were presumably flattened during the Holocene interstadial.

Similarly to what observed for the GVF, the morphological asset of the TVF suggests the occurrence of a diffuse monogenetic volcanism, which however does not support the presence of a large common magmatic reservoir, as also confirmed by petrological studies of volcanic samples collected in the region (Rotolo et al., 2006).

CONCLUSION

High-resolution bathymetric data and ROV images allowed new detailed morphological analysis of the present-day setting of the Graham submarine volcanic field located offshore southwestern Sicily.

Another volcanic field, the TVF, was also identified on the adjacent Terribile Bank and analyzed.

The relationship between the morphology of the seamounts and underwater volcanic processes proved the monogenetic nature of this volcanism, which is part of a wider and scattered volcanism affecting the northwestern Sicily Channel. This volcanism represents a peculiarity, since it took place outside of the typical geodynamic settings of other fields such as subduction or oceanic rift zones, and far from long-lived volcanic systems.

The ten of cones forming the GVF is likely the witnesses of a Late Pleistocene to Holocene submarine volcanism. This age is reasonably hypothesized by means of the analysis of some morphological parameters (i.e., depth and shape of the tops, presence and depth of abrasion and depositional terraces, level of erosive dismantlement) in relationship with sea-level fluctuations and taking into account analogies with the post-eruptive morphological evolution of Ferdinandea shoal formed during the 1831 eruption and other volcanic seamounts worldwide, such as the satellite shoals of Surtsey formed during the 1963–67 eruption.

The shape of the seamounts and their distribution within the GVF attested to the interaction between volcanism and tectonics in the formation of the field itself. The overall N-S trend of the volcanic field reflects the orientation of the Capo Granitola-Sciacca transpressive transfer zone, which favored the volcanism in this region. The cones within the fields are generally grouped into clusters or merged to form coalesced edifices, both aligned along NW-SE to WNW-ESE preferential directions, consistent with the main regional tectonic structures associated with the Plio-Quaternary continental rifting of the Sicily Channel.

This paper could furnish a key to better understand the volcano-tectonic complexity of this region and provide a useful comparison for other submarine areas affected by monogenetic volcanism.

The improvement of the knowledge of this shallow submarine volcanism would be also of great interest in determining volcanic risk in the area.

DATA AVAILABILITY STATEMENT

The datasets generated for this study are available on request to the corresponding author.

AUTHOR CONTRIBUTIONS

DC processed the multibeam bathymetric data. DC and MC conceived and designed the research and acquired the multibeam bathymetric data and ROV images, interpreted the dataset integrating it with the available information concerning the study area and conceived the morphological evolutional of the Graham volcanic field, discussing methods, analyses, results and conclusion of the manuscript.

ACKNOWLEDGMENTS

We thank for their contribution during the "Ferdinandea 2012" research cruise, the captain of the R/V ASTREA Massimo Saporito and his crew, Simone Pietro Canese and the C.L.C. Luigi Manzueto of ISPRA, and Andrei Diaconov of SoProMar. Moreover, we are grateful to Alessandro Bosman of CNR for his support during the multibeam data processing and to our colleague William Moreland for improving the English style. Finally, we are grateful to the Chief Editor Valerio Acocella,

Guest Associate Editor GG and two reviewers for providing useful suggestions in improving the manuscript quality. The oceanographic cruise "Ferdinandea 2012" was supported by "Studi e Ricerche" 2012-grant of INGV-Osservatorio Etneo.

SUPPLEMENTARY MATERIAL

The Supplementary Material for this article can be found online at: https://www.frontiersin.org/articles/10.3389/feart.2019.00311/full#supplementary-material

REFERENCES

Antonioli, F., Donadio, C., Ferranti, L., Margottini, C., and De Vita, A. (1994). Il Banco Graham: storia, sismica storica, petrologia e geomorfologia subacquea. Nascita e scomparsa del vulcano sommerso nel Canale di Sicilia. *Mem. Descr. Carta Geol. d'It.* 52, 99–102.

Aranda-Gómez, J. J., Luhr, J. F., Housh, T. B., Connor, C. B., Becker, T., and Henry, C. D. (2003). Synextensional pliocene–pleistocene eruptive activity in the camargo volcanic field, Chihuahua, México. *Geol. Soc. Am. Bull.* 115, 289–313.

Arena, F., Laface, V., Malara, G., Romolo, A., Viviano, A., Fiamma, V., et al. (2015). Wave climate analysis for the design of wave energy harvesters in the Mediterranean Sea. *Renew. Energy* 77, 125–141. doi: 10.1016/j.renene.2014.12.002

Argnani, A. (1990). The Strait of Sicily rift zone: foreland deformation related to the evolution of a backarc basin. *J. Geodyn.* 12, 311–331. doi: 10.1016/0264-3707(90)90028-s

Baker, E. T., Massoth, G. J., de Ronde, C. E. J., Lupton, J. E., and McInnes, B. I. A. (2002). Observation sand sampling of an ongoing subsurface eruption of Kavachi volcano, Solomon Islands, May 2000. *Geology* 30, 975–978.

Beccaluva, L., Colantoni, P., Di Girolamo, P., and Savelli, C. (1981). Upper Miocene submarine volcanism in the Strait of Sicily (Banco Senza Nome). *Bull. Volcanol.* 44, 573–581. doi: 10.1007/bf02600587

Boccaletti, M., Cello, G., and Tortorici, L. (1987). Transtensional tectonics in the Sicily Channel. *J. Struct. Geol.* 9, 869–876. doi: 10.1016/0191-8141(87)90087-3

Bottari, C., Stiros, S. C., and Teramo, A. (2009). Archaeological evidence for destructive earthquakes in Sicily between 400 B.C. and A.D. 600. *Geoarchaeology* 24, 147–175. doi: 10.1002/gea.20260

Bruce, P. M., and Huppert, H. E. (1989). Thermal control of basaltic fissure eruptions. *Nature* 342, 665–667. doi: 10.1038/342665a0

Burollet, P. F., Mugniot, J. M., and Sweeney, P. (1978). "The geology of the pelagian block: the margins and basins of southern Tunisia and Tripolitania," in *The Ocean Basins and Margins. The Western Mediterranean*, Vol. 4b, eds A. E. M. Nairn, W. H. Kanes, and F. G. Stelhi, (New York, NY: Plenum), 331–359. doi: 10.1007/978-1-4684-3039-4_6

Calanchi, N., Colantoni, P., Rossi, P. L., Saitta, M., and Serri, G. (1989). The Strait of Sicily continental rift systems: physiography and petrochemistry of the submarine volcanic centres. *Mar. Geol.* 87, 55–83. doi: 10.1016/0025-3227(89)90145-X

Calò, M., and Parisi, L. (2014). Evidences of a Lithospheric fault zone in the Sicily Channel (Southern Italy) from instrumental seismicity data. *Geophys. J. Int.* 199, 219–225. doi: 10.1093/gji/ggu249

Cañón-Tapia, E. (2016). Reappraisal of the significance of volcanic fields. *J. Volcanol. Geotherm. Res.* 310, 26–38. doi: 10.1016/j.jvolgeores.2015.11.010

Cas, R. A. F., and Giordano, G. (2014). Submarine volcanism: a review of the constraints, processes and products, and relevance to the cabo de gata volcanic succession. *Ital. J. Geosci.* 133, 362–377. doi: 10.3301/ijg.2014.46

Cas, R. A. F., Landis, C. A., and Fordyce, E. (1989). A monogenetic, surtla-type, surtseyan volcano from the eocene-oligocene waiareka-deborah volcanics, otago, New Zealand: a model. *Bull. Volcanol.* 51, 281–298. doi: 10.1007/bf01073517

Casalbore, D., Falese, F., Martorelli, E., Romagnoli, C., and Chiocci, F. L. (2017). Submarine depositional terraces in the Tyrrhenian Sea as a proxy for paleo-sea level reconstruction: problems and perspective. *Q. Int.* 439, 169–180. doi: 10.1016/j.quaint.2016.07.051

Casalbore, D., Romagnoli, C., Pimentel, A., Quartau, R., Casas, D., Ercilla, G., et al. (2015). Volcanic, tectonic and mass-wasting processes offshore Terceira island (Azores) revealed by high-resolution seafloor mapping. *Bull. Volcanol.* 77:24. doi: 10.1007/s00445-015-0905-3

Cavallaro, D., Monaco, C., Polonia, A., Sulli, A., and Di Stefano, A. (2017). Evidence of positive tectonic inversion in the north-central sector of the Sicily Channel (Central Mediterranean). *Nat. Hazards* 86, S233–S251. doi: 10.1017/s11069-016-2515-6

Civile, D., Lodolo, E., Accaino, F., Geletti, R., Schiattarella, M., Giustiniani, M., et al. (2018). Capo granitola-sciacca fault zone (Sicilian Channel, Central Mediterranean): structure vs magmatism. *Mar. Pet. Geol.* 96, 627–644. doi: 10.1016/j.marpetgeo.2018.05.016

Civile, D., Lodolo, E., Alp, H., Ben-Avraham, Z., Cova, A., Baradello, L., et al. (2014). Seismic stratigraphy and structural setting of the Adventure Plateau (Sicily Channel). *Mar. Geophys. Res.* 35, 37–53. doi: 10.1007/s11001-013-9205-5

Civile, D., Lodolo, E., Tortorici, L., Lanzafame, G., and Brancolini, G. (2008). Relationships between magmatism and tectonics in a continental rift: the Pantelleria Island region (Sicily Channel, Italy). *Mar. Geol.* 251, 32–46. doi: 10.1016/j.margeo.2008.01.009

Civile, D., Lodolo, E., Zecchin, M., Ben-Avraham, Z., Baradello, L., Accettella, D., et al. (2015). The lost adventure archipelago (Sicilian Channel, Mediterranean Sea): morpho-bathymetry and late quaternary palaeogeographic evolution. *Glob. Planet. Change* 125, 36–47. doi: 10.1016/j.gloplacha.2014.12.003

Clague, D. A., Moore, J. G., and Reynolds, J. R. (2000a). Formation of submarine flat-topped volcanic cones in Hawaii. *Bull. Volcanol.* 62, 214–233. doi: 10.1007/s004450000088

Clague, D. A., Reynolds, J. R., and Davis, A. S. (2000b). Near ridge seamount chains in the northeastern Pacific Ocean. *J. Geophys. Res.* 105, 16541–16561. doi: 10.1029/2000jb900082

Clark, P. U., Dyke, A. S., Shakun, J. D., Carlson, A. E., Clark, J., Wohlfarth, B., et al. (2009). The last glacial maximum. *Science* 325, 710–714. doi: 10.1126/science.1172873

Colantoni, P. (1975). Note di geologia marina sul Canale di Sicilia. *Giorn. Geol.* 40, 181–207.

Colantoni, P., Del Monte, M., Gallignani, P., and Zarudzky, E. F. K. (1975). Il Banco Graham: un vulcano recente nel Canale di Sicilia. *Giorn. Geol.* 40, 141–162.

Coltelli, M., Cavallaro, D., D'Anna, G., D'Alessandro, A., Grassa, F., Mangano, G., et al. (2016). Exploring the submarine graham bank in the sicily channel. *Ann. Geophys.* 59:S0208. doi: 10.4401/ag-6929

Conte, A. M., Martorelli, E., Calarco, M., Sposato, A., Perinelli, C., Coltelli, M., et al. (2014). The 1891 submarine eruption offshore Pantelleria Island (Sicily Channel, Italy): identification of the vent and characterization of products and eruptive style. *Geochem. Geophys. Geosyst.* 15, 2555–2574. doi: 10.1002/2014GC005238

Corazzato, C., and Tibaldi, A. (2006). Fracture control on type, morphology and distribution of parasitic volcanic cones: an example from Mt. Etna Italy. *J. Volcanol. Geotherm. Res.* 158, 177–194. doi: 10.1016/j.jvolgeores.2006.04.018

Corcoran, P. L., and Moore, L. N. (2008). Subaqueous eruption and shallow-water reworking of a small-volume Surtseyan edifice at Kakanui, New Zealand. *Can. J. Earth Sci.* 45, 1469–1485. doi: 10.1139/e08-068

Corti, G., Cuffaro, M., Doglioni, C., Innocenti, F., and Manetti, P. (2006). Coexisting geodynamic processes in the Sicily Channel. *Geol. Soc. Am. Spec. Pap.* 409, 83–96.

Cowell, P. J., Hanslow, D. J., and Meleo, J. F. (1999). "The shoreface," in *Handbook of Beach and Shoreface Morphodynamics*, ed. A. D. Short, (Chichester: Wiley and Sons), 39–71.

Dean, D. R. (1980). Graham island, charles lyell, and the craters of elevation controversy. *Isis* 71, 571–588. doi: 10.1086/352593

Di Geronimo, I., Rosso, A., and Sanfilippo, R. (1993). "The corallium rubrum fossiliferous banks off sciacca (Strait of Sicily)," in *Il Corallo Rosso in Mediterraneo: Arte, Storia e Scienza*, eds F. Cicogna, and R. Cattaneo Vietti (Roma: Ministero Risorse Agricole Alimentari Forestali), 75–107.

Drago, A., Sorgente, R., and Olita, A. (2010). Sea temperature, salinity and total velocity climatological fields for the south-central Mediterranean Sea. GCP/RER/010/ITA/MSM-TD-14. *MedSudMed Tech. Doc.* 14:35.

Falautano, G., Falzone, G., Lanzafame, G., Macaluso, D., Niosi, M., and Rossi, P. (2010). *Primi Tentativi di monitoraggio dei resti sottomarini dell'eruzione che nel 1831 costruì l'Isola Ferdinandea nel Canale di Sicilia. Rapporti tecnici INGV*. Rome: Istituto Nazionale di Geofisica e Vulcanologia.

Falzone, G., Lanzafame, G., and Rossi, P. L. (2009). Il vulcano Ferdinandea nel Canale di Sicilia. *Geoitalia* 29, 15–20.

Favalli, M., Karátson, D., Mazzarini, F., Pareschi, M. T., and Boschi, E. (2009). Morphometry of scoria cones located on a volcano flank: a case study from Mt. Etna (Italy), based on high-resolution LiDAR data. *J. Volcanol. Geotherm. Res.* 186, 320–330. doi: 10.1016/j.jvolgeores.2009.07.011

Fedorik, J., Toscani, G., Lodolo, E., Civile, D., Bonini, L., and Seno, S. (2018). Structural analysis and Miocene-to-Present tectonic evolution of a lithospheric-scale, transcurrent lineament: the Sciacca Fault (Sicilian Channel, Central Mediterranean Sea). *Tectonophysics* 722, 342–355. doi: 10.1016/j.tecto.2017.11.014

Ferranti, L., Pepe, F., Barreca, G., Meccariello, M., and Monaco, C. (2019). Multi-temporal tectonic evolution of Capo Granitola and Sciacca foreland transcurrent faults (Sicily Channel). *Tectonophysics* 765, 187–204. doi: 10.1016/j.tecto.2019.05.002

Fleming, K., Johnston, P., Zwartz, D., Yokoyama, Y., Lambeck, K., and Chappell, J. (1998). Refining the eustatic sea-level curve since the Last Glacial Maximum using far- and intermediate-field sites. *Earth Planet. Sci. Lett.* 163, 327–342. doi: 10.1016/s0012-821x(98)00198-8

Foutrakis, P. M., and Anastasakis, G. (2018). Bathy-morphological setting of the submarine pausanias volcanic field, south aegean active volcanic arc. *J. Maps* 14, 341–347. doi: 10.1080/17445647.2018.1473816

Gemmellaro, C. (1831). *Relazione dei fenomeni del nuovo vulcano sorto dal mare fra la costa di Sicilia e l'Isola di Pantelleria nel mese di luglio 1831*. Catania: ne' torchi della Regia Università Carmelo Pastore 48:25.

Ghisetti, F. C., Gorman, A. R., Grasso, M., and Vezzani, L. (2009). Imprint of foreland structure on the deformation of a thrust sheet. The Plio-Pleistocene Gela Nappe (southern Sicily, Italy). *Tectonics* 28:TC4015. doi: 10.1029/2008TC002385

Global Volcanism Program (2013a). *Campi Flegrei del Mar di Sicilia (211070) in Volcanoes of the World, 4.7.6*, ed. E. Venzke, (Washington, DC: Smithsonian Institution), doi: 10.5479/si.GVP.VOTW4-2013

Global Volcanism Program (2013b). *Izu-Oshima (284010) in Volcanoes of the World, 4.7.6*, ed. E. Venzke, (Washington, DC: Smithsonian Institution), doi: 10.5479/si.GVP.VOTW4-2013

Green, A. N., Cooper, J. A. G., and Salzmann, L. (2014). Geomorphic and stratigraphic signals of postglacial meltwater pulses on continental shelves. *Geology* 42, 151–154. doi: 10.1130/g35052.1

Guidoboni, E., Muggia, A., Marconi, C., and Boschi, E. (2002). A case study in archaeoseismology. The collapses of the Selinunte temples (Southwestern Sicily): two earthquakes identified. *Bull. Seismol. Soc. Am.* 92, 2961–2982. doi: 10.1785/0120010286

Head, J. W., Wilson, L., and Smith, D. K. (1996). Mid-ocean ridge eruptive vent morphology and substructure: evidence for the dike widths, eruption rates, and axial volcanic ridges. *J. Geophys. Res.* 101, 28265–28280. doi: 10.1029/96jb02275

Hernàndez-Molina, F. J., Fernàndez-Salas, L. M., Lobo, F. J., Somoza, L., Díaz del Río, V., and Alveirinho Dias, J. M. (2000). The infralittoral prograding wedge: a new largescale progradational sedimentary body in shallow marine environments. *Geo Mar. Lett.* 20, 109–117. doi: 10.1007/s003670000040

Jakobsson, S. P., Gudmundsson, G., and Moore, J. G. (2000). Geological monitoring of Surtsey, Iceland, 1967–1998. *Surtsey Res.* 11, 99–108.

Jakobsson, S. P., Thors, K., Vésteinsson, Á. T., and Ásbjörnsdóttir, L. (2009). Some aspects of the seafloor morphology at Surtsey volcano: the new multibeam bathymetric survey of 2007. *Surtsey Res.* 12, 9–20.

Jongsma, D., Van Hinte, J. E., and Woodside, J. M. (1985). Geologic structure and neotectonics of the North African continental margin south of Sicily. *Mar. Pet. Geol.* 2, 156–179. doi: 10.1016/0264-8172(85)90005-4

Kereszturi, G., and Németh, K. (2012). "Monogenetic basaltic volcanoes: genetic classification, growth, geomorphology and degradation," in *Updates in Volcanology New Advances in Understanding Volcanic Systems*, ed. K. Németh, (Rijeka: InTech), doi: 10.5772/51387

Kokelaar, B. P. (1983). The mechanism of surtseyan volcanism. *J. Geol. Soc. Lond.* 140, 939–944. doi: 10.1144/gsjgs.140.6.0939

Kokelaar, B. P. (1986). Magma–water interactions in subaqueous and emergent basaltic volcanism. *Bull. Volcanol.* 48, 275–289. doi: 10.1007/bf01081756

Kokelaar, B. P., and Durant, G. P. (1983). The submarine eruption and erosion of Surtla (Surtsey), Iceland. *J. Volcanol. Geotherm. Res.* 19, 239–246. doi: 10.1016/0377-0273(83)90112-9

Lambeck, K., Antonioli, F., Anzidei, M., Ferranti, L., Leoni, G., Scicchitano, G., et al. (2011). Sea level change along the Italian coast during the Holocene and projections for the future. *Quat. Int.* 232, 250–257. doi: 10.1016/j.quaint.2010.04.026

Latter, J. H. (1981). Tsunamis of volcanic origin. *Bull. Volcanol.* 44, 467–490. doi: 10.1007/BF02600578

Liu, J. P., and Milliman, J. D. (2004). Reconsidering melt-water pulses 1A and 1B: global impacts of rapid sea-level rise. *J. Ocean Univ. China* 3, 183–190. doi: 10.1007/s11802-004-0033-8

Lodolo, E., Civile, D., Zanolla, C., and Geletti, R. (2012). Magnetic signature of the Sicily Channel volcanism. *Mar. Geophys. Res.* 33, 33–44. doi: 10.1007/s11001-011-9144-y

Lodolo, E., Civile, D., Zecchin, M., Zampa, L. S., and Accaino, F. (2019a). A series of volcanic edifices discovered a few kilometers off the coast of SW Sicily. *Mar. Geol.* 416:105999. doi: 10.1016/j.margeo.2019.105999

Lodolo, E., Zampa, L., and Civile, D. (2019b). The Graham and Terrible volcanic province (NW Sicilian Channel): gravimetric constraints for the magmatic manifestations. *Bull. Volcanol.* 81:17. doi: 10.1007/s00445-019-1274-0

Lodolo, E., Sanfilippo, R., Rajola, G., Canese, S., Andaloro, F., Montagna, P., et al. (2017). The red coral deposits of the Graham Bank area: constraints on the Holocene volcanic activity of the Sicilian Channel. *Geo. Res. J.* 13, 126–133. doi: 10.1016/j.grj.2017.04.003

Lucchi, F., Ricchi, A., Romagnoli, C., Casalbore, D., and Quartau, R. (2019). Late Quaternary paleo sea level geomorphological markers of opposite vertical movements at Salina volcanic island (Aeolian Arc). *Earth Surf. Process. Landforms* 44, 2377–2395. doi: 10.1002/esp.4651

Machado, F., Parsons, W. H., Richards, A. F., and Mulford, J. W. (1962). Capelinhos eruption of Fayal Volcano, Azores, 1957–1958. *J. Geophys. Res.* 67, 3519–3529. doi: 10.1029/jz067i009p03519

Marzolla, B. (1831). *Descrizione dell'Isola Ferdinandea al mezzogiorno della Sicilia*. Napoli: Reale Officio Topografico.

McClinton, T., White, S. M., Colman, A., and Sinton, J. M. (2013). Reconstructing lava flow emplacement processes at the hot spot-affected Galápagos Spreading Center, 95° W and 92° W. *Geochem. Geophys. Geosyst.* 14, 2731–2756. doi: 10.1002/ggge.20157

Mercalli, G. (1883). *Geologia d'Italia: Vulcani e fenomeni vulcanici*. Milano: Vallardi editore.

Mitchell, N. C., Masselink, G., Huthnance, J. M., Fernàndez-Salas, L. M., and Lobo, F. J. (2012a). Depths of modern coastal sand clinoforms. *J. Sed. Res.* 82, 469–481. doi: 10.2110/jsr.2012.40

Mitchell, N. C., Stretch, R., Oppenheimer, C., Kay, D., and Beier, C. (2012b). Cone morphologies associated with shallow marine eruptions: east Pico Island, Azores. *Bull. Volcanol.* 74, 2289–2301. doi: 10.1007/s00445-012-0662-5

Mitchell, N. C., Stretch, R., Tempera, F., and Ligi, M. (2016). "Volcanism in the Azores: a marine geophysical perspective," in *Volcanoes of the Azores*, eds U. Kueppers, and C. Beier, (Berlin: Springer-Verlag).

Moore, J. G., Jakobsson, S. P., and Hólmjárn, J. (1992). Subsidence of Surtsey volcano, 1967–1991. *Bull. Volcanol.* 55, 17–24. doi: 10.1007/bf00301116

Muscheler, R., Kromer, B., Bjorck, S., Svensson, A., Friedrich, M., Kaiser, K. F., et al. (2008). Tree rings and ice cores reveal 14C calibration uncertainties during the Younger Dryas. *Nat. Geosci.* 1, 263–267. doi: 10.1038/ngeo128

Németh, K. (2010). "Monogenetic volcanic fields: origin, sedimentary record, and relationship with polygenetic volcanism," in *What Is a Volcano?*, eds E. Canon-Tapia, and A. Szakacs, (Boulder, CO: Geological Society of America), 43–66. doi: 10.1130/2010.2470(04)

Németh, K., and Kereszturi, G. (2015). Monogenetic volcanism: personal views and discussion. *Int. J. Earth Sci.* 104, 2131–2146. doi: 10.1007/s00531-015-1243-6

Norrman, J. O., and Erlingsson, U. (1992). The submarine morphology of Surtsey volcanic group. *Surtsey Res. Prog. Rep.* 10, 45–56.

Paris, R., Wassmer, P., Sartohadi, J., Lavigne, F., Barthomeuf, B., Desgages, E., et al. (2009). Tsunamis as geomorphic crises: lessons from the December 26, 2004 tsunami in Lhok Nga, West Banda Aceh (Sumatra, Indonesia). *Geomorphology* 104, 59–72. doi: 10.1016/j.geomorph.2008.05.040

Pensa, A., Pinton, A., Vita, L., Bonamico, A., De Benedetti, A. A., and Giordano, G. (2019). ATLAS of italian submarine volcanic structures. *Mem. Descr. Carta Geol. d'It.* 104, 77–183.

Quartau, R., Hipolito, A., Romagnoli, C., Casalbore, D., Madeira, J., Tempera, F., et al. (2014). The morphology of insular shelves as a key for understanding the geological evolution of volcanic islands: insights from Terceira Island (Azores). *Geochem. Geophys. Geosyst.* 15, 1801–1826. doi: 10.1002/2014gc005248

Quartau, R., Trenhaile, A. S., Mitchell, N. C., and Tempera, F. (2010). Development of volcanic insular shelves: insight from observations and modelling of Faial Island in the Azores Archipelago. *Mar. Geol.* 275, 66–83. doi: 10.1016/j.margeo.2010.04.008

Ramalho, R. S., Quartau, R., Trenhaile, A. S., Mitchell, N. C., Woodroffe, C. D., and Ávila, S. P. (2013). Coastal evolution on volcanic oceanic islands: a complex interplay between volcanism, erosion, sedimentation, sea-level change and biogenic production. *Earth Sci. Rev.* 127, 140–170. doi: 10.1016/j.earscirev.2013.10.007

Rappaport, Y., Naar, D. F., Barton, C. C., Liu, Z. J., and Hey, R. N. (1997). Morphology and distribution of seamounts surrounding Easter Island. *J. Geophys. Res.* 102, 24713–24728. doi: 10.1029/97jb01634

Reuther, C. D., Ben-Avraham, Z., and Grasso, M. (1993). Origin and role of major strike-slip transfers during plate collision in the central Mediterranean. *Terra Nova* 5, 249–257. doi: 10.1111/j.1365-3121.1993.tb00256.x

Rivera, J., Lastras, G., Canals, M., Acosta, J., Arrese, B., Hermida, N., et al. (2013). Construction of an oceanic island: insights from the El Hierro (Canary Islands) 2011–2012 submarine volcanic eruption. *Geology* 41, 355–358. doi: 10.1130/G33863.1

Romagnoli, C., and Jakobsson, S. P. (2015). Post-eruptive morphological evolution of island volcanoes: surtsey as a modern case study. *Geomorphology* 250, 384–396. doi: 10.1016/j.geomorph.2015.09.016

Romero Ruiz, C., García-Cacho, L., Araña, V., Yanes Luque, A., and Felpeto, A. (2000). Submarine volcanism surrounding Tenerife, Canary Islands: implications for tectonic controls, and oceanic shield forming processes. *J. Volcanol. Geotherm. Res.* 103, 105–119. doi: 10.1016/s0377-0273(00)00218-3

Rotolo, S. G., Castorina, F., Cellura, D., and Pompilio, M. (2006). Petrology and geochemistry of submarine volcanism in the Sicily Channel Rift. *J. Geol.* 114, 355–365. doi: 10.1086/501223

Salzmann, L., Green, A., and Cooper, J. A. G. (2013). Submerged barrier shoreline sequences on a high energy, steep and narrow shelf. *Mar. Geol.* 346, 366–374. doi: 10.1016/j.margeo.2013.10.003

Schmidt, R., and Schmincke, H. U. (2002). From seamount to oceanic island, Porto Santo, central east-Atlantic. *Int. J. Earth Sci.* 91, 594–614. doi: 10.1007/s00531-001-0243-x

Siddall, M., Rohling, E. J., Almogi-Labin, A., Hemleben, C., Meischner, D., Schmelzer, I., et al. (2003). Sea-level fluctuations during the last glacial cycle. *Nature* 423, 853–858. doi: 10.1038/nature01690

Siebe, C., Komorowski, J. C., Navarro, C., McHone, J. Z., Delgado, H., and Cortes, A. (1995). Submarine eruption near Socorro Island, Mexico: geochemistry and scanning electron microscopy studies of floating scoria and reticulite. *J. Volcanol. Geotherm. Res.* 68, 239–271. doi: 10.1016/0377-0273(95)00029-1

Sinapi, L., Lamberti, L. O., Pizzeghello, N. M., and Ivaldi, R. (2016). The Graham Bank: hydrographic features and safety of navigation. *Int. Hydrogr. Rev.* 15, 7–20.

Spatola, D., Micallef, A., Sulli, A., Basilone, L., Ferreri, R., Basilone, G., et al. (2018). The Graham Bank (Sicily Channel, central Mediterranean Sea): seafloor signatures of volcanic and tectonic controls. *Geomorphology* 318, 375–389. doi: 10.1016/j.geomorph.2018.07.006

Stretch, R., Mitchell, N. C., and Portaro, R. A. (2006). A morphometric analysis of the submarine volcanic ridge of Pico Island. *J. Volcanol. Geotherm. Res.* 156, 35–54. doi: 10.1016/j.jvolgeores.2006.03.009

Sturkell, E., Einarsson, P., Geirsson, H., Tryggvason, E., Moore, J. G., and Ólafsdóttir, R. (2009). Precision levelling and geodetic GPS observations performed on Surtsey between 1967 and 2002. *Surtsey Res.* 12, 39–74.

Tempera, F., Hipolito, A., Madeira, J., Vieira, S., Campos, A., and Mitchell, N. C. (2013). Condor seamount (Azores, NE Atlantic): a morphotectonic interpretation. *Deep Sea Res. Part II Top. Stud. Oceanogr.* 98, 7–23. doi: 10.1016/j.dsr2.2013.09.016

Thorarinsson, S. (1967). *Surtsey. The New Island in the North Atlantic*. New York, NY: Viking Press Inc.

Tibaldi, A. (1995). Morphology of pyroclastic cones and tectonics. *J. Geophys. Res.* 100, 24521–24535. doi: 10.1029/95jb02250

Torelli, L., Grasso, M., Mazzoldi, G., Peis, D., and Gori, D. (1995). Cretaceous to Neogene structural evolution of the Lampedusa shelf (Pelagian Sea, Central Mediterranean). *Terra Nova* 7, 200–212. doi: 10.1111/j.1365-3121.1995.tb00689.x

Trenhaile, A. S. (1989). Sea level oscillations and the development of rock coasts. *Elsevier Oceanogr. Ser.* 49, 271–295. doi: 10.1016/s0422-9894(08)70129-6

Trenhaile, A. S. (2000). Modeling the development of wave-cut shore platforms. *Mar. Geol.* 166, 163–178. doi: 10.1016/s0025-3227(00)00013-x

Trenhaile, A. S. (2001). Modelling the Quaternary evolution of shore platforms and erosional continental shelves. *Earth Surf. Process. Landforms* 26, 1103–1128. doi: 10.1002/esp.255

Valentine, G. A., and Connor, C. B. (2015). "Basaltic volcanic fields," in *Encyclopedia of Volcanoes*, 2nd Edn, eds H. Sigurdsson, B. F. Houghton, S. R. McNutt, H. Rymer, and J. Stix, (London: Academic Press), 423–439. doi: 10.1016/b978-0-12-385938-9.00023-7

Vaughan, R. G., and Webley, P. W. (2010). Satellite observations of a surtseyan eruption: hunga Ha'apai. *Tonga. J. Volcanol. Geotherm. Res.* 198, 177–186. doi: 10.1002/2017GL076621

Washington, H. S. (1909). The submarine eruption of 1831 and 1891 near Pantelleria. *Am. J. Sci.* 27, 131–150. doi: 10.2475/ajs.s4-27.158.131

Wessel, P., Sandwell, D. T., and Kim, S. S. (2010). The global seamount census. *Oceanography* 23, 24–33. doi: 10.5670/oceanog.2010.60

Weston, F. S. (1964). List of recorded volcanic eruptions in the Azores with brief reports. *Bol. Mus. Lab. Min. Geol. Face Ciên Lisboa* 10, 3–18.

White, J. D. L. (1996). Pre-emergent construction of a lacustrine basaltic volcano, Pahvant Butte, Utah (USA). *Bull. Volcanol.* 58, 249–262. doi: 10.1007/s004450050138

White, J. D. L., and Houghton, B. (2000). "Surtseyan and related phreatomagmatic eruptions," in *Encyclopedia of Volcanoes*, ed. H. Sigurdsson, (London: Academic Press), 495–511.

Zecchin, M., Ceramicola, S., Gordini, E., Deponte, M., and Critelli, S. (2011). Cliff overstep model and variability in the geometry of transgressive erosional surfaces in high-gradient shelves: the case of the Ionian Calabrian margin (southern Italy). *Mar. Geol.* 281, 43–58. doi: 10.1016/j.margeo.2011.02.003

Zecchin, M., Ceramicola, S., Lodolo, E., Casalbore, D., and Chiocci, F. L. (2015). Episodic, rapid sea-level rises on the central Mediterranean shelves after the last glacial maximum: a review. *Mar. Geol.* 369, 212–223. doi: 10.1016/j.margeo.2015.09.002

Conflict of Interest: The authors declare that the research was conducted in the absence of any commercial or financial relationships that could be construed as a potential conflict of interest.